CHALMERS

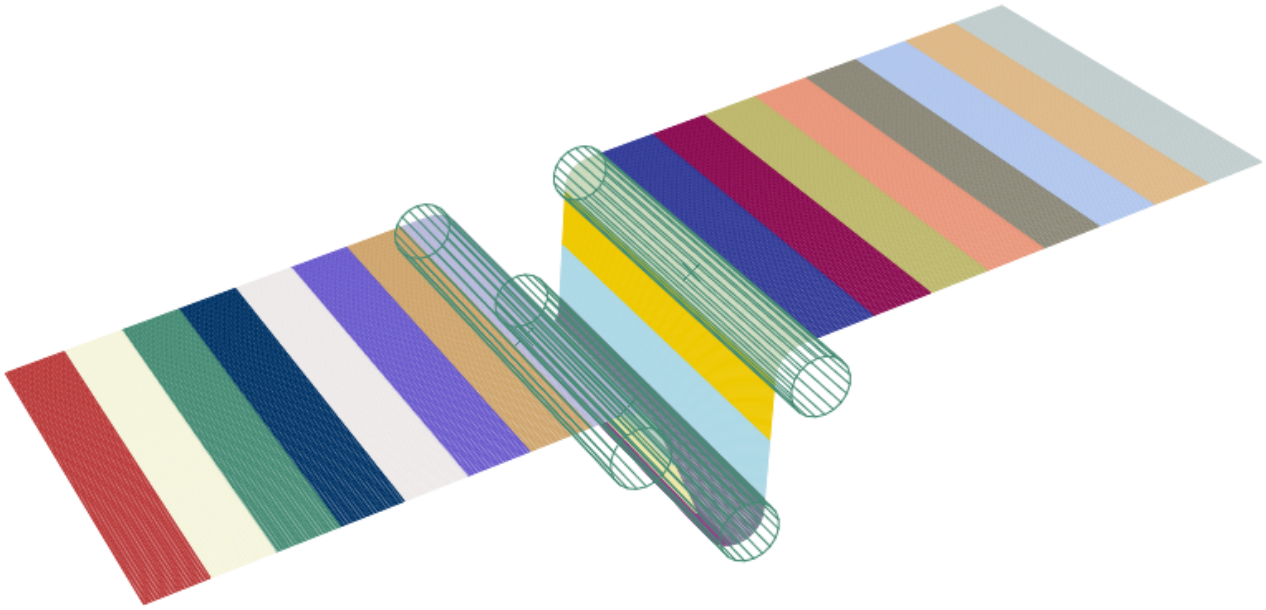

A comparison of finite element formulations for analysis of the converting process of packaging materials

Master's thesis in Applied Mechanics

SUSANNA LINDBERG
PATRIK SANDVIK

Department of Applied Mechanics
Division of Material and Computational Mechanics
CHALMERS UNIVERSITY OF TECHNOLOGY
Göteborg, Sweden 2015
Master's thesis 2015:10

MASTER'S THESIS IN APPLIED MECHANICS

A comparison of finite element formulations for analysis of the converting process of packaging materials

SUSANNA LINDBERG
PATRIK SANDVIK

Department of Applied Mechanics

Division of Material and Computational Mechanics

CHALMERS UNIVERSITY OF TECHNOLOGY

Göteborg, Sweden 2015

A comparison of finite element formulations for analysis of the converting process of packaging materials
SUSANNA LINDBERG
PATRIK SANDVIK

Master's thesis 2015:10
ISSN 1652-8557
Department of Applied Mechanics
Division of Material and Computational Mechanics
Chalmers University of Technology
SE-412 96 Göteborg
Sweden
Telephone: +46 (0)31-772 1000

Cover:
The web motion set-up using periodic media analysis

Chalmers Reproservice
Göteborg, Sweden 2015

A comparison of finite element formulations for analysis of the converting process of packaging materials
Master's thesis in Applied Mechanics
SUSANNA LINDBERG
PATRIK SANDVIK
Department of Applied Mechanics
Division of Material and Computational Mechanics
Chalmers University of Technology

Abstract

Packaging industry supplies a variety of different carton packages to their customers in the food and beverage industries. Packaging industry also develops and produces packaging material. One key aspect of the production of the packaging material is the converting process, where the lamination of the core material, paperboard, takes place. To improve the quality of the produced packaging material it is important to understand the converting process. To deepen the knowledge about the converting process, simulation tools are used to investigate how the process affects the packaging material. The company is continuously working on improving its abilities on simulations. This thesis investigates new methods, apart from those used today, that can be used to simulate parts of the converting process. All performed simulations are based on the finite element method and created in the commercial software Abaqus.

The first part of the converting process that is studied is a web motion problem where paperboard is transported over idle rollers. This is a key aspect of the converting process and the company has had some difficulties with their simulations of the web motion. Non-converging finite element analyses and failure to reach steady state in the paperboard flow are some displayed problems with the current model. The other part of the converting process that is studied is the nip in the lamination process. At the lamination nip, a steel roller and a roller consisting of a steel core and a rubber coating, are forced together. The industry wants to have a simple, thin model of the lamination nip, from where the contact pressure in the nip and the temperature distribution throughout the rubber are sought for. The model used today is somewhat complicated and demands a lot of manual labor why a more simple model is desired.

For the web handling problem, two different methods are investigated. An Eulerian approach is studied where the element mesh is fixed in space and the paperboard is allowed to flow through the mesh. By using Eulerian inflow and outflow boundary conditions the paperboard may flow in and out of the mesh freely and thus the modeled paperboard may be shortened to reduce the model size. The other approach investigated is an Abaqus functionality called periodic media analysis. The paperboard is then divided into building blocks which are reused in the analysis, meaning that the model size may be reduced to improve calculation time. For the lamination nip, an Eulerian approach is once more considered. The rubber is then modeled using the Eulerian approach, allowing for a finer mesh at the nip and a more coarse mesh where only rotation of the roller occurs.

It was shown that the Eulerian approach resulted in infeasible run times for the web handling problem wherefore further studies of this model are not recommended. The periodic media model on the other hand displays some potentially good qualities such as mesh reduction. However, uneven stresses in the paperboard and inaccurate contact pressure are obtained. Based on these findings, this method is recommended for analyses where the paperboard is not the main part of interest. Further studies on this approach are needed. Also the Eulerian approach for the lamination nip needs further investigations. The key factors for an good setup where identified but no such model was created.

Keywords: FEM, Abaqus, Explicit, Web handling, Lamination nip, Eulerian modeling, Periodic Media Analysis

Preface

In this theses method development two different finite element modeling formulations have been investigated. This thesis work has been conducted at FS Dynamics during fall 2014 and the project definition has been formulate together with a company acting in the packaging industry. First of all we would like to thank our supervisor Svetlana Lebedeva at FS Dynamics for all her support throughout the project and for her ideas of how to proceed when we got stuck. We would aslo like to thank Fredrik Karström at FS Dynamics. We also send out thanks to all colleagues at FS Dynamics, who made us feel like a part of the group from day one. We would also like to send our gratitudes to Robert Lillbacka, Mattias Månsson and Jiri Havir for giving us the opportunity to write this thesis. Our special thanks goes to our examiner Magnus Ekh from the division of Material and Computational Mechanics at Chalmers University of Technology. Last but not least want to thank all our friends and family for their patience and for always being there.

Contents

1 Introduction

This thesis has been conducted in collaboration with a company that supplies a variety of different paperboard packaging to their customers in the food and beverage industries. Complete processing and packaging solutions are provided, including service and installation of machines at customer plants. The company also develops and produces their own packaging material. The packaging material consists of mainly three materials; polyethylene for avoiding leakage, aluminum to prevent the light from affecting the content and paperboard for stiffness of the package. Figure 1.1 displays an example of the layup of a packaging material.

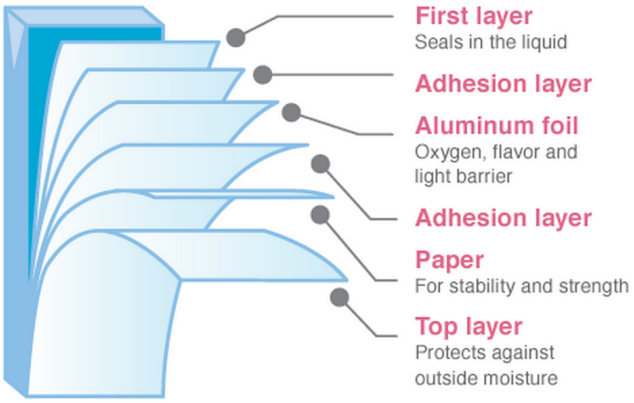

Figure 1.1: Example of packaging material (Milkunleashed 2014)

It is critical that the packaging material meets the customers' demands. One of the key aspects of the company's manufacturing technology is the converting process, where the packaging material is produced. By identifying and understanding the underlying factors that affect the converting process, the production of packaging material may be improved. This may lead to an improved productivity and a higher quality of the produced packaging material.

The converting process is a multiple step process where a base material, the paperboard in Figure 1.1, is turned into the final packaging material. One important aspect of the converting process is the continuous rolling of the material, where the material is guided through the machine by the use of rollers, a problem called web motion. Another important aspect of the converting process is the lamination processes, where the polyethylene and the aluminum is added to the paperboard. Figure 1.2a displays a schematic view of the web motion, while Figure 1.2b displays a schematic view of the lamination process.

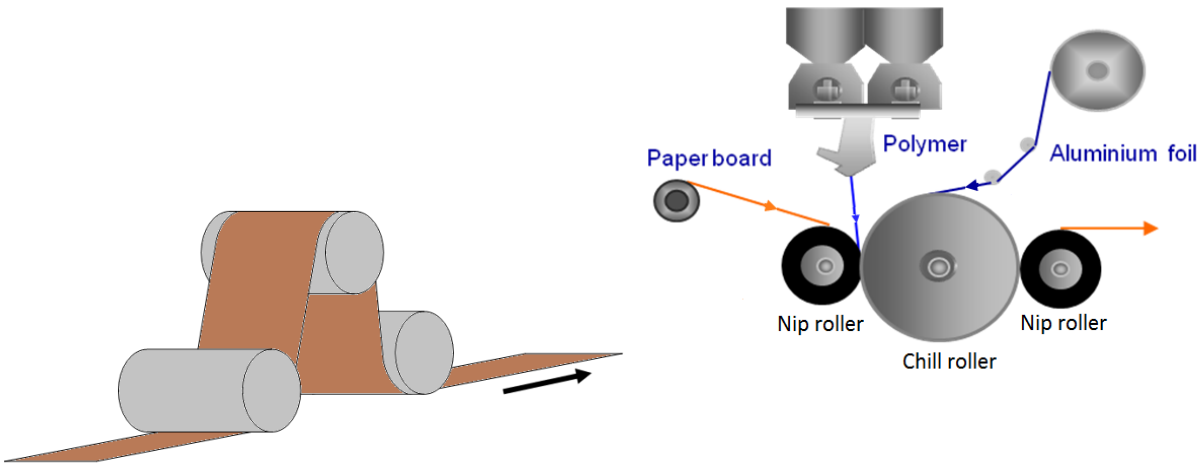

(a) Web motion in the converting process *(b) Lamination in the converting process*

Figure 1.2: Display of two key aspects in the converting process

Numerical simulations are a valuable tool when studying the converting process. Various numerical analyses, using for example the finite element method (FEM), are performed to gain more knowledge about the converting process. Web motion and the lamination process are two such problems analyzed using FEM. It has been shown difficult to simulate the web motion and the lamination process in a satisfactory manner using a Lagrangian formulation. Therefore, this thesis will investigate whether it is possible to simulate these processes using other formulations available in the commercial finite element software Abaqus.

1.1 Problem definition

In the converting process, the paperboard runs over idle rollers between the lamination stations. It is important that the paperboard is transported over the rollers without getting damaged. For this reason it is of interest to know the impact this web motion problem has on the paperboard. An example of a question that is addressed is how the paperboard response will be to a nonaligned roller. Furthermore, at the end of the converting process, the finished packaging material is cut into thinner stripes and rolled onto separate rolls. To separate the material after it has been cut, the paperboard runs over a cambered roller. How this cambered roller affects the packaging material is also a question for the packaging industry.

The finite element modeling of the web motion is today performed using a Lagrangian approach. Thus, a Lagrangian (or material) frame of reference is used where the finite element mesh is fixed to the paperboard (Irgens 2008). When simulating the web motion, a steady state solution is sought for. The company defines steady state as when the paperboard travels with the correct velocity and the rollers rotates with such angular velocity that no slip occurs between the paperboard and the rollers (except at the end of the contact region where slip will occur). With the current model it has been proven hard to reach steady state in the simulations.

A large amount of paperboard needs to travel through the rollers before steady state is reached. The effect of using a Lagrangian approach is that the whole piece of paperboard that is to be analyzed is created prior to the analysis. Thus, the piece of paperboard that needs to be created becomes long if steady state is to be reached. As a consequence, a large number of elements are needed and the finite element analysis becomes computationally heavy. It is only in the proximity of the rollers that the paperboard response is interesting, why the long paperboard leads to a lot of excess data. Figure 1.3 displays an example of how the initial setup might look like for an Lagrangian analysis.

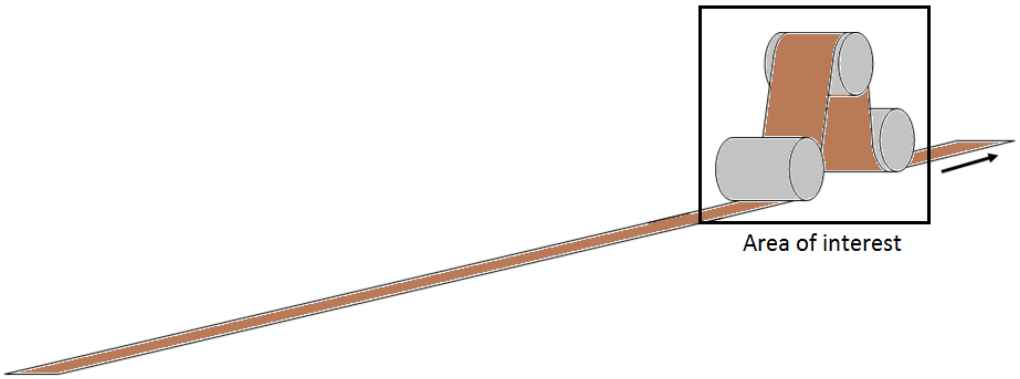

Figure 1.3: Example of how an initial setup may look like when a Lagrangian approach is used. A long piece of paperboard needs to be created if steady state is to be reached

The Lagrangian model developed by the company has not reached steady state even though simulations have been running for several weeks. Therefore, they are looking for alternative methods to simulate the web motion problem where steady state is reached and the calculation time is reduced.

One interesting aspect in the lamination process is the nip that occurs between the chill- and nip rollers, see Figure 1.2b. The chill roller has the purpose to cool down the melted polyethylene. The lamination nip that the nip rollers generate, has the purpose of removing entrapped air and create adhesion between the different layers of the packaging material. The nip rollers are composed of a steel core covered with rubber. The material properties of the rubber is affected by temperature why it is of interest to obtain the temperature distribution throughout the rubber. The contact pressure in the lamination nip is of importance to study.

The finite element model the company has developed is two-dimensional and designed to obtain the contact pressure between the nip- and chill roller as well as the temperature distribution in the rubber. The obtained data is used in larger models as input when performing simulations of larger parts of the lamination process. The current model is complicated and even though the run time is acceptable according to the company, the model requires a lot of manual labor and iterations. Therefore, the company wants to investigate whether it is possible to create a similar two-dimensional model using another method which requires less manual work.

1.2 Objective

The objective of the thesis is to investigate whether it is possible to simulate the described web motion and the lamination nip using other finite element formulations than the Lagrangian.

1.3 Methodology of thesis

As a first attempt an Eulerian approach is studied for both the web motion and the lamination nip. This means that an Eulerian (or spatial) frame of reference is used (Irgens 2008). Thus, the finite element mesh is fixed in space and the material is allowed to flow through the mesh. This approach allows the mesh to be finer where it is particularly interesting to get accurate data. The Eulerian approach also allows for an inflow and outflow of material in the mesh. Hence, for the web motion problem, the paperboard length may be reduced since material is created during the analysis.

For the web motion problem an additional method is investigated as well. The method is based on a functionality provided in Abaqus called Periodic media analysis. The Periodic media analysis utilizes a Lagrangian approach but the functionality allows for a shorter paperboard model since the paperboard is reused in the analysis. Thus the model size, in terms of number of nodes, is reduced significantly. Initially in the project, a literature study is conducted. The literature study includes both scientific papers and Abaqus manuals.

The commercial software Abaqus will be used to perform the simulations and the focus in this thesis is on the investigation of new methods. Thus, no optimizations of the models are performed.

1.4 Thesis Outline

The thesis starts with an introduction, presenting the thesis problem definition, objective and methodology of thesis. After the introduction, a theoretical framework is presented. The theoretical framework includes essential theories in the finite element method as well as descriptions of the relevant functionalities provided in Abaqus. This is followed by a chapter covering the web motion problem and one chapter for the lamination nip. Here descriptions of the tested models are presented as well as the obtained results from the simulations of the different models. Finally, concluding remarks and recommendations completes the thesis.

2 Theoretical framework

This chapter gives a theoretical background to introduce the reader to the topic. One of the main sources used is the Abaqus 6.14-1 manuals together with articles on relevant topics.

2.1 Fundamental concepts

The finite element method is the numerical analysis technique used in the thesis through the commercial finite element software Abaqus. FEM is a commonly used discretization method where the domain is divided into sub-domains, or elements, for which a problem is easier to solve. The basic theories in FEM is not presented in the thesis but the reader is referred to literature such as Zienkiewicz and Taylor (1991a); Ottosen and Petersson (1992).

2.1.1 Implicit and explicit methods for dynamic problems

A problem can be defined as dynamic if at least one of the following statements applies; the response is affected by mass inertia, the time history response is important, or the frequency of applied loading is higher than a fifth of the lowest eigenfrequency (Brolin 2014). The problems studied in this thesis are to be considered dynamic since mass inertia and time history are key aspects of the problems. When solving a dynamic problem using FEM, the time dimension has to be considered as well (Zienkiewicz and Taylor 1991b, Chapter 9).

A matrix differential equation governing a variety of dynamic problems is formulated in Chapter 9 in Zienkiewicz and Taylor (1991b). A system of ordinary differential equations with the characteristic form (Daping and Yanchao 2013; Zienkiewicz and Taylor 1991b) is obtained:

$$\boldsymbol{M}\ddot{\boldsymbol{u}} + \boldsymbol{C}\dot{\boldsymbol{u}} + \boldsymbol{K}\boldsymbol{u} = \boldsymbol{f} \tag{2.1}$$

where $\boldsymbol{M}$ is the mass matrix, $\boldsymbol{C}$ is the damping matrix, $\boldsymbol{K}$ the stiffness matrix, $\boldsymbol{f}$ is the time-dependent load vector and $\boldsymbol{u}$ contains nodal displacements. The matrices and vectors are assembled by the usual rule from element sub-matrices (Zienkiewicz and Taylor 1991b).

For cases when equation (2.1) is linear, it is often solved by using the often cost-effective modal integration method, which is described in Chapter 2.5 in the *Abaqus Theory Guide* (2014). However, in reality non-linearities are often present and the equation system must instead be solved using a direct time integrating method. The equation system is non-linear if, for example, any of the matrices are displacement dependent according to $\boldsymbol{M} = \boldsymbol{M}(\boldsymbol{u})$, $\boldsymbol{C} = \boldsymbol{C}(\boldsymbol{u})$ and $\boldsymbol{K} = \boldsymbol{K}(\boldsymbol{u})$. In addition, transient problems on linear systems are generally not economical to be treated as the static linear problems either (Zienkiewicz and Taylor 1991b). Thus, if equation (2.1) is non-linear or the problem is transient, the solution is obtained through a discretization process applied directly in the time domain (Zienkiewicz and Taylor 1991b, Chapter 10). That is, the solution is obtained through a direct time integration of all degrees of freedom of the FE-model (*Abaqus Theory Guide* 2014, Chapter 2.4).

The direct time integration methods of equation (2.1) may be divided into implicit or explicit schemes (*Abaqus Theory Guide* 2014, Chapter 2.4). When applying an explicit scheme, the dynamic quantities at the next time step, $t + \Delta t$, are calculated based only on the quantities obtained in the previous time step, t (*Abaqus Theory Guide* 2014). However, an implicit scheme implies that the dynamic quantities at the next time step, $t + \Delta t$, are calculated based on not only the quantities obtained in the previous time step, t, but also on the quantities obtained at the time step, $t + \Delta t$ (*Abaqus Theory Guide* 2014).

The implicit approach

There are many implicit operators used for time integration of dynamic problems. Two common ones are the Hilber-Hughes-Taylor operator and the backward Euler operator (*Abaqus Theory Guide* 2014). The state variables in equation (2.1) are calculated for each time increment. To ensure convergence of the solution, a convergence criterion is used in the analysis. If convergence is not reached, the time increment is modified and a new solution on the new time increment is obtained and again checked if acceptable. One criterion used to check if the obtained solution has converged is called the *half-increment residual*, which is utilized in Abaqus/Standard, the Abaqus implicit solver (*Abaqus Theory Guide* 2014). The half-increment residual thus provides a measure of the accuracy of the obtained solution for a given time step. If the residual is too high, a smaller time increment is needed and if the residual is small the time increment may be increased. The algorithm is described in Chapter 7.2.4 of the *Abaqus Analysis User's Guide* (2014). For further reading, see Hibbitt and Karlsson (1979), where the method is introduced.

The explicit approach

The central difference approximation is a commonly used explicit integration tool and is implemented in the explicit solver in Abaqus, Abaqus/Explicit (Daping and Yanchao 2013; *Abaqus Theory Guide* 2014). The core of the central difference approximation is to substitute the displacement differentials with the following expressions (Daping and Yanchao 2013):

$$\ddot{\boldsymbol{u}}_t = \frac{\boldsymbol{u}_{t-\Delta t} - 2\boldsymbol{u}_t + \boldsymbol{u}_{t+\Delta t}}{\Delta t^2} \tag{2.2}$$

$$\dot{\boldsymbol{u}}_t = \frac{\boldsymbol{u}_{t+\Delta t} - \boldsymbol{u}_{t-\Delta t}}{2\Delta t} \tag{2.3}$$

Zienkiewicz and Taylor (1991b) discuss in Chapter 10 several methods for solving equation (2.1) explicitly. Single step methods, multistep methods and non-linearities are covered. One key aspect is however that the mass matrix $\boldsymbol{M}$ and the damping matrix $\boldsymbol{C}$ in equation (2.1) are assumed to be diagonal (lumped) to obtain an explicit solution of the equation (Zienkiewicz and Taylor 1991b).

From equations (2.2) and (2.3) it is seen that the time increment used will influences the stability of the solution as well as the computational time cost. In fact, the central difference approximation is conditionally stable (Zienkiewicz and Taylor 1991b; *Abaqus Theory Guide* 2014; Daping and Yanchao 2013).

Since the central difference operator is conditionally stable, the size of the time increment in an explicit solver must be limited (*Abaqus Theory Guide* 2014). The stability limit for the largest time increment correlates with the time required for a stress wave to pass through the smallest element dimension in the FE-model (*Abaqus Theory Guide* 2014). This means that the smaller the elements are and the faster the stress waves is, the smaller time increment is needed. The time increment is calculated as (*Abaqus Theory Guide* 2014):

$$\Delta t \leq \Delta t_{lim} = min\left(\pi \frac{L}{C}\right) \tag{2.4}$$

where L is a characteristic element dimension closely corresponding with the element's minimum edge length, and:

$$C = \sqrt{\frac{\hat{\lambda} + 2\hat{\mu}}{\rho}}, \tag{2.5}$$

where the Lamé constants $\hat{\lambda}$ and $\hat{\mu}$ can be expressed in terms of Poisson's ratio ν and Young's modulus E as follows:

$$\hat{\lambda} = \frac{E\nu}{(1+\nu)(1-2\nu)} \quad and, \quad \hat{\mu} = \frac{E}{2(1+\nu)}$$

Furthermore, C is here the current effective dilatational wave speed of the material and ρ is the density. Daping and Yanchao (2013) is defining the critical time increment differently by using the speed of sound in the material defined as:

$$C = \sqrt{\frac{E}{(1-\nu^2)\rho}} \tag{2.6}$$

In Chapter 2.4.5 in the *Abaqus Theory Guide* (2014), an example of an explicit solution is given. The material has no damping wherefore the damping matrix $\boldsymbol{C}$ is ignored. The acceleration is calculated in the current step as:

$$\ddot{\boldsymbol{u}}^i = \boldsymbol{M}^{-1} \cdot (\boldsymbol{f}^i - \boldsymbol{I}^i) \tag{2.7}$$

where $\boldsymbol{M}$ is the diagonal lumped mass matrix, $\boldsymbol{f}$ is the external force vector, $\boldsymbol{I}$ is the internal force vector containing the displacements and i denotes the increment number. When using the explicit procedure, no iterations and no tangent stiffness matrix are needed for the calculations. By using the diagonal element mass matrices, the inversion of $\boldsymbol{M}$ is triaxial which is beneficial for the computational efficiency (*Abaqus Theory Guide* 2014). When the acceleration at increment i is solved for, the displacement at increment $i+1$ may be calculated through the central difference approximation. First the velocity of the displacement at increment $i+\frac{1}{2}$ is solved for:

$$\dot{\boldsymbol{u}}^{i+\frac{1}{2}} = \dot{\boldsymbol{u}}^{i-\frac{1}{2}} + \frac{\Delta t^{i+1} + \Delta t^i}{2} \ddot{\boldsymbol{u}}^i \tag{2.8}$$

and thus the displacement at increment $i+1$ is obtained as:

$$\boldsymbol{u}^{i+1} = \boldsymbol{u}^i + \Delta t^{i+1} \dot{\boldsymbol{u}}^{i+\frac{1}{2}} \tag{2.9}$$

Advantages and disadvantages of the implicit and explicit approach

Implicit schemes display good characteristics when used for low-speed dynamic problems, linear dynamic problems or problems where small non-linearities exists (*Abaqus Theory Guide* 2014). However, implicit schemes will encounter convergence problem for problems characterized by very discontinuous short-term events (Sun, K. Lee, and H. Lee 1999), cases where stress wave propagation is involved, highly non-linear problems (Yongsheng Qi and Zhou 2013) and transient problems (*Abaqus Theory Guide* 2014).

Since the explicit scheme only make one iteration for each time increment, it is very cost effective for each time increment. However, due to the condition of the time increment, this may become small and thus many calculations might be needed. In such cases, an implicit scheme is preferred. The cost for solving the non-linear equations with the explicit scheme rises linearly with model size increase, whereas for the implicit scheme the cost rises more rapidly (Sun, K. Lee, and H. Lee 1999). For this reason it is preferable to use an explicit scheme for large problems.

Sun, K. Lee, and H. Lee (1999) have compared solving dynamic problems using implicit or explicit methods and concluded that the implicit method is advantageous when a slow contact problem is solved. When the problem is slow, the high frequency numerical noise in the solution plays an important role. This is filtered by a small numerical damping, which is introduced in the implicit method. For faster contact problems, the numerical damping lowers the amplitudes of the results making the explicit method the favorable. For such problems, the explicit method is also more cost efficient (Sun, K. Lee, and H. Lee 1999).

2.1.2 Eulerian and Lagrangian approach

There are two fundamentally different ways of describing the motion in continuum mechanics (Irgens 2008). One approach is to look at the problem from points fixed in space. Thus, all quantities in this description are a function of position in space. This description is called Eulerian, or spatial, description of motion (Irgens 2008). The other description is called Lagrangian, or material, description of motion. This means that the motion is described through the same material points in one body throughout the analysis. All quantities in this description are thus functions of the material points (Irgens 2008).

The motion described in a Lagrangian manner can be formulated as $\boldsymbol{\phi} = \boldsymbol{\phi}(\boldsymbol{X}, t)$, where $\boldsymbol{X}$ is a reference position, typically the original position, and t is the time. $\boldsymbol{\phi}$ is used as an arbitrary solution variable (Davidson 2013). When a Lagrangian FE-model is created, the mesh is fixed to the material and therefore deforms with the material. When adopting a Lagrangian approach, the material is well defined in space throughout the analysis. In solid mechanics this is the most common way of constructing a model (Irgens 2008).

The three conservation equations for mass, momentum and energy, written in a Lagrangian manner are listed below (Davidson 2013):

$$\frac{\mathrm{d}\rho}{\mathrm{d}t} + \rho \bigtriangledown \cdot \boldsymbol{v} = 0 \tag{2.10}$$

$$\rho \frac{\mathrm{d}\boldsymbol{v}}{\mathrm{d}t} = \bigtriangledown \cdot \boldsymbol{\sigma} + \rho \boldsymbol{b} \tag{2.11}$$

$$\frac{\mathrm{d}E}{\mathrm{d}t} = \bigtriangledown \cdot (\boldsymbol{\sigma} \cdot \boldsymbol{v}) + \rho \boldsymbol{b} \cdot \boldsymbol{v} \Rightarrow \left\{ E = \frac{1}{2} \rho \boldsymbol{v} \cdot \boldsymbol{v} + e \right\} \Rightarrow \frac{\mathrm{d}e}{\mathrm{d}t} = \boldsymbol{\sigma} : \boldsymbol{D} \tag{2.12}$$

The Eulerian motion is usually described by a function depending on a chosen fixed position, $\boldsymbol{x}$, through which the material passes (Davidson 2013). The function can also depend on time, $\boldsymbol{\phi} = \boldsymbol{\phi}(\boldsymbol{x}, t)$. Since $\boldsymbol{\phi}$ depends on both fixed positions and time, the function must be expressed both in space and time, wherefore the spatial derivative $\frac{\partial \phi}{\partial t}$ is used. An Eulerian FE-model is characterized by the fact that the material flows through the mesh while the mesh is fixed in space.

The relation between the Lagrangian description of motion and the Eulerian description of motion is clearly seen when comparing the material time derivative (Benson and Okazawa 2003):

$$\frac{\mathrm{d}\phi}{\mathrm{d}t} = \frac{\partial \phi}{\partial t} + \boldsymbol{v} \cdot (\bigtriangledown \phi) = \frac{\partial \phi}{\partial t} + \boldsymbol{v} \frac{\partial \phi}{\partial \boldsymbol{x}} \tag{2.13}$$

where $\boldsymbol{v}$ is the velocity of the material. The left hand side is the Lagrangian description while the right hand side displays the Eulerian description. The Eulerian description consists of one spatial term, which describes the variation of $\boldsymbol{\phi}$ in time at position $\boldsymbol{x}$, and one convective rate of change term, which describes the variation of $\boldsymbol{\phi}$ in space when it passes the position $\boldsymbol{x}$ (Davidson 2013).

With the use of equation (2.13), the Lagrangian conservation equations (2.10)-(2.12) can be transfered into Eulerian conservation equations (2.14)-(2.16):

$$\frac{\partial \rho}{\partial t} + \boldsymbol{v} \cdot (\bigtriangledown \rho) + \rho \bigtriangledown \cdot \boldsymbol{v} = 0 \tag{2.14}$$

$$\frac{\partial \boldsymbol{v}}{\partial t} + \boldsymbol{v} \cdot (\bigtriangledown \cdot \boldsymbol{v}) = \frac{1}{\rho}(\bigtriangledown \cdot \boldsymbol{\sigma}) + \boldsymbol{b} \tag{2.15}$$

$$\frac{\partial e}{\partial t} + \boldsymbol{v} \cdot (\bigtriangledown e) = \boldsymbol{\sigma} : \boldsymbol{D} \tag{2.16}$$

Large distortions in the mesh may be obtained in large deformation analyses using the Lagrangian approach. Therefore, in analysis where large deformations occurs it may be beneficial to use Eulerian formulations since the elements do not deform and the material can flow freely across the element edges. The Eulerian code also has the advantage of allowing turbulent flow (Benson 1992). Since the body is not fixed to the Eulerian mesh, new material boundaries are freely created when an Eulerian approach is used (Ghosh and Kikuchi 1991).

The Eulerian approach is limited when it comes to spatial resolution of the material boundaries (Benson and Okazawa 1987). This means that surfaces of material are not as accurately created compared to the Lagrangian material boundaries. Thus, the Lagrangian approach results in a more accurate contact definition since the occurrence of material is better defined. According to Ghosh and Kikuchi (1991) the Eulerian approach may be ill-suited for domains where boundaries and interfaces move substantially. Another drawback regarding the Eulerian approach is that only one integration point in each Eulerian element exists, why several element thicknesses are required to adequately represent bending (Benson and Okazawa 1987).

The convective term in the Eulerian formulation may cause numerical difficulties (Draganis 2014; Wing Kam Liu and Chang 1986). The absence of convective term in the Lagrangian approach is an advantage (Ghosh and Kikuchi 1991). The Lagrangian approach satisfies less complex governing equations as well and simple updating techniques for path and history dependent materials are other advantages (Ghosh and Kikuchi 1991).

2.1.3 Rayleigh material damping

It is hard to fully establish the source of damping in materials since there often is a combination of multiple sources (*Abaqus Analysis User's Guide* 2014). A variety of methods are available in Abaqus to specify damping that models the energy loss in a dynamic system. One common model used for material damping was developed by Lord Rayleigh and is known as Rayleigh damping, which is the model used in Abaqus for general damping (*Abaqus Analysis User's Guide* 2014, Chapter 26.1.1). The damping matrix is found in the governing equation, 2.1, where it is denoted $\boldsymbol{C}$. When using Rayleigh damping, this can be expressed as (Orcina 2014a):

$$\boldsymbol{C} = \alpha \boldsymbol{M} + \beta \boldsymbol{K} \tag{2.17}$$

where $\boldsymbol{M}$ and $\boldsymbol{K}$ are the system mass and stiffness matrices respectively. α and β are predefined constants where α is called the mass proportional damping constant with unit 1/time while β is the stiffness proportional damping constant with unit time. These constants are usually estimated from experience and by using an iterative approach. The fraction of critical damping in the material, ξ, is illustrated by the blue line in Figure 2.1 and is formulated as (*Abaqus Analysis User's Guide* 2014):

$$\xi = \frac{\alpha}{2\omega} + \frac{\beta \omega}{2} \tag{2.18}$$

where ω is one natural frequency in radians per second and ξ is the fraction of critical damping. It can be noted that the mass proportional damping dominates for lower frequencies while the stiffness damping dominates for higher frequencies.

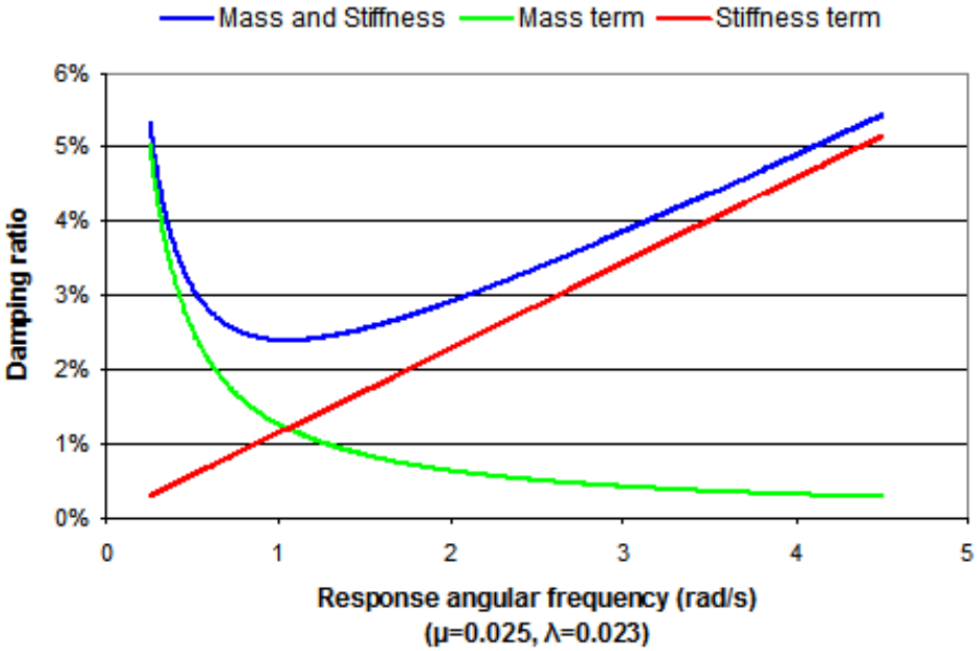

Figure 2.1: Influence of mass (green) and stiffness (red) proportional coefficients in Rayleigh damping where the blue line shows the total damping if both mass and stiffness damping coefficients are used (Orcina 2014b)

2.2 Description of adequate functionalities supported in Abaqus

SIMULIA Abaqus is a program developed by Dassault Systemès (DassaultSystemès 2014) used for solving finite element problems. In this project, Abaqus version 6.14-1 is used. In this section two methods used in this project are introduced. The first method described is used for both the web motion and the lamination nip and is an Eulerian method. The other method presented is called periodic media analysis and is used for the web motion analysis.

2.2.1 Eulerian analysis in Abaqus

In an Eulerian analysis, the material flows through the mesh and an explicit time integration is applied. Chapter 14 in *Abaqus Analysis User's Guide* (2014) describes how Eulerian modeling is used in Abaqus. The time incrementation algorithm is known as Lagrange-plus-remap and consists of two phases. The first phase is a Lagrangian where the mesh deforms with the material. This is followed by the Eulerian phase where the mesh is re-meshed to the original position while the material is fixed in space (*Abaqus Analysis User's Guide* 2014). The amount of material in an element is described by the Eulerian volume fraction where the percentage of material within each element is computed in each step. Since the elements do not always consist of 100% material, the surfaces are approximated and not consistent. Rectangular-shaped elements provide the best accuracy and performance in Eulerian analyses (*Abaqus Verification Guide* 2014, Chapter 3.19.1). In Abaqus 6.14-1 anisotropic material models can be used where the material orientation is remapped as the material passes the element faces (*Abaqus Release Notes* 2014).

For Eulerian modeling in Abaqus the possible element types are limited to two different multi-material elements,

the standard element EC3D8R and an element with thermal coupling, EC3D8RT (*Abaqus Analysis User's Guide* 2014, Chapter 14.1). These elements have eight nodes, which implies that only three dimensional analyses can be performed. The elements uses a reduced integration scheme with one integration point and hourglass effects are controlled.

The interactions between two different Eulerian material instances are modeled with a sticky contact. If the contact between two bodies is important it is more accurate to model one of the materials with Lagrangian elements. Such a method is called coupled Eulerian-Lagrangian, where the parts modeled with Eulerian elements typically undergo large deformations while the Lagrangian parts often are less deformed (*Abaqus Analysis User's Guide* 2014). Eulerian contact does not support analytical rigid surfaces.

One drawback with Eulerian modeling is that displacements cannot be prescribed, but instead velocity or acceleration are prescribed to control the material flow. General surface loading can not be used, instead distributed loads such as pressure can be applied (*Abaqus Analysis User's Guide* 2014). Eulerian boundary conditions can be applied to control the inflow and outflow of material but once the material is outside of the mesh it is lost (*Abaqus Analysis User's Guide* 2014).

It is not possible to import Eulerian elements into second analyses, neither is the import of Eulerian-Lagrangian contact states supported (*Abaqus Analysis User's Guide* 2014). Initial conditions on the other hand can be used. Another disadvantage is that fine mesh resolution might be required in Eulerian analyses, resulting in small time increments and long simulation times. Mass scaling is not supported for Eulerian elements.

2.2.2 Web Motion Modeled with Periodic Media Analysis

Periodic media analysis is an Abaqus Explicit functionality which uses a Lagrangian approach but where the the material created is reused in the analysis. When having very large meshes that are repetitive, this method can be used to reduce the run time. The mesh is divided into a number of identical parts called building blocks. When the mesh is moving and a certain block passes a defined trigger plane, the block in the end of the chain (outlet) is transfered to the beginning of the chain (inlet) and the data is transfered from the previous inlet block to the current inlet block. Figure 2.2 taken from an Abaqus example illustrates the building block transfer process.

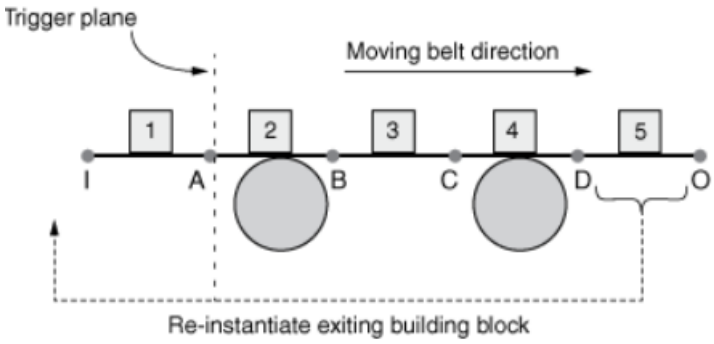

*Figure 2.2: An illustation of how the shuffling process is done. When the inlet nodes, here marked with I, passes the trigger plane the last building block is shuffled to be the new inlet block (*Abaqus Verification Guide *2014, Chapter 3.15)*

Since the mesh is always moving and the nodes changes position, the boundary conditions cannot be applied directly to the nodes in the mesh. Instead the boundary conditions are specified at two reference nodes which are connected to the inlet and outlet edges. The only valid boundary condition is velocity and the only load that can be applied is a concentrated force.

The periodic media function connects all the building blocks using a tie constrain. To reduce the influence of the

small chock that occurs when two blocks are tied in the shuffling process, it is recommended to add mass-material damping. The periodic media analysis has the limitations that neither a coupled Eulerian-Lagrangian contact nor the contact pair algorithm can be used. Instead, a general contact can be applied. It is also important that the distance between the inlet and outlet blocks only differs by a translation in one direction. The elements that can be used within the building blocks are membranes, shells, trusses, continuum elements and rigid elements (*Abaqus Analysis User's Guide* 2014).

3 Introducing Eulerian modeling by looking at a flat piece of paperboard

To understand how the functionalities of the Eulerian modeling technique in Abaqus works, a simple model consisting of a flat piece of paperboard, modeled in an Eulerian domain, is created. The pre- and post-processing of the model are performed in Abaqus/CAE. The chapter starts with a closer description of the model whereupon the results from the different tests are presented. The tests are conducted with the purpose that the analyses should give insight about the modeling technique in areas related to the web motion and the nip problems that are to be studied in this thesis. Initially, a test illustrating the flow of material through the Eulerian domain is conducted. After that, simulations related to velocity and tension in the paperboard are ran. Finally, a contact problem is constructed to investigate the contact properties between an Eulerian paperboard and a Lagrangian plate.

3.1 The Eulerian paperboard model

When adapting an Eulerian modeling technique, an Eulerian domain is created initially. To create an Eulerian part within the domain, the elements are assigned the part's material where the part is supposed to be positioned. Elements that are not assigned any material in particular are assigned to contain void. The Eulerian elements may contain multiple materials which implies that an element may be assigned a specific material between 0% and 100%.

There are mainly two different methods to assign material to the Eulerian elements in Abaqus/CAE. It is possible to create or import a part in Abaqus/CAE, project it in the Eulerian domain and let Abaqus/CAE calculate where the material is to be assigned in the Eulerian domain. An alternative method is to create a set in the Eulerian domain with the dimensions of the part that is to be created. This set may then be used in Abaqus/CAE to be filled with the material and thus create the part in the Eulerian domain. For simple geometries, the latter alternative is proved to be a faster approach.

The Eulerian paperboard model consists of an Eulerian domain and one material, paperboard. For simplicity the paperboard is modeled using an isotropic linear elastic material model. The paperboard has an inlet and an outlet in the Eulerian domain where different boundary conditions are applied. A figure of this model, when it is cut in half, is displayed in Figure 3.1. The cut is in the lengthwise direction and is made to present the paperboard within the Eulerian domain. Table 3.1 shows the material properties and model dimensions used in the model.

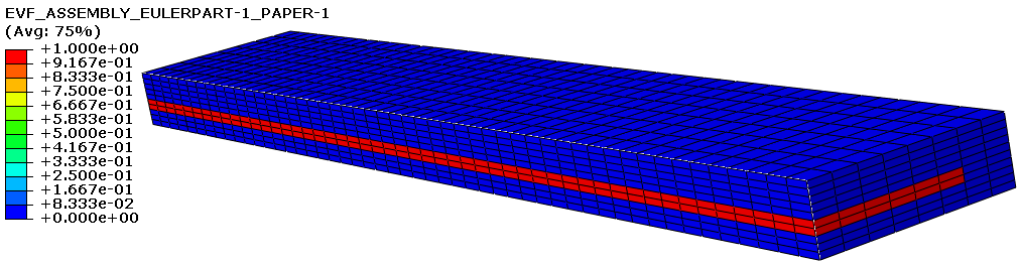

Figure 3.1: An Eulerian paperboard model. The legend shows the volume fraction of material within each element. Elements colored red are 100% filled with paperboard while elements colored blue contains of void

Table 3.1: Material properties and dimensions of the paperboard (denoted with the subscript pb) and dimensions of the Eulerian domain (subscript Ed). $l \times w \times t$ represent the length, width and thickness of the paperboard, Eulerian domain or of the element (subscript el)

E_{pb}	9000	[MPa]
ν_{pb}	0.2	
ρ_{pb}	6.56×10^{-4}	[g/mm^3]
$l_{pb} \times w_{pb} \times t_{pb}$	50×10×0.5	[mm]
$l_{Ed} \times w_{Ed} \times t_{Ed}$	50×14×2.5	[mm]
$l_{el} \times w_{el} \times t_{el}$	1.0×1.0×0.25	[mm]

There are four different initial conditions that are combined into different configurations; (1) the paperboard is stress free and has no velocity, (2) the paperboard is stress free but has a velocity of 10 m/s in the longitudinal direction, (3) the paperboard is subjected to a tensile stress of 2 MPa in the lengthwise direction, but no velocity, and (4) the paperboard is under tensile stress of 2 MPa while it has a velocity of 10 m/s in the longitudinal direction.

Various boundary conditions are applied on the inlet and outlet surfaces of the Eulerian domain. As a consequence of applying the boundary conditions on the inlet and outlet surfaces of the Eulerian domain, the inlet and outlet surfaces of the paperboard are affected by the boundary conditions. The purpose of the Eulerian boundary conditions are to let the paperboard flow in and out of the Eulerian domain freely. In addition, there is a pressure load applied to the inlet surface. The purpose of this load is to maintain or ramp up a tensile stress in the paperboard. On the outlet surface, a velocity boundary condition is applied. This is to either maintain a initial velocity of the material or to ramp up a velocity of the material.

When analyzing the tests on the flat plate model, the velocities and stresses in the material are studied. A reference point is chosen in the center of the paperboard in which variables are analyzed. Figure 3.2 displays this point which is called RP1 from here on.

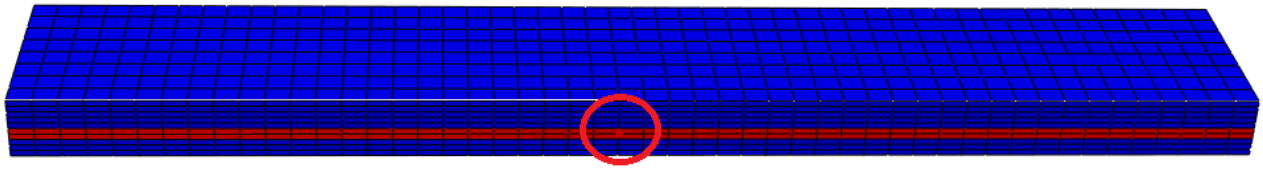

Figure 3.2: The chosen reference point, RP1, in the Eulerian mesh

To illustrate the flow of material through the mesh, a test is conducted on the flat plate model. The setup is that the velocity initial condition is applied to the paperboard and throughout the simulation the velocity is held constant by the velocity boundary condition on the outlet surface. Hence, a flow of material in the Eulerian domain is created. To present the flow, the Eulerian boundary condition void is applied on the inlet surface so no additional paperboard is created. Thus, it is easy to show the flow of paperboard through the Eulerian mesh. Figure 3.3 displays the paperboard flow where Figure 3.3a illustrates the initial setup while Figure 3.3b illustrates the position of the paperboard after 2.5 ms of the simulation.

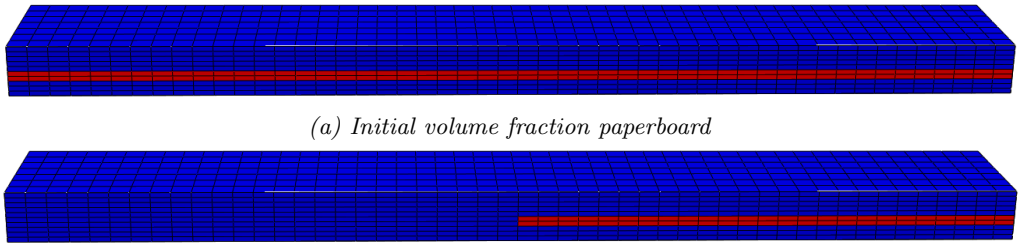

(a) Initial volume fraction paperboard

(b) Volume fraction of paperboard after 2.5 ms of flow

Figure 3.3: Illustration of the flow of paperboard through mesh

3.1.1 Analysis of the effects on the paperboard due to velocity conditions

In the lamination nip and web motion applications, flow of material through the Eulerian domain occurs. Therefore, it is of interest to look further into how the movement of the paperboard through the Eulerian domain affects the paperboard and thus, such tests are performed. Questions that are investigated are: Is it possible to hold a constant flow of material through the mesh? Is it possible to ramp up a flow of material from a stationary initial condition? What is the stress response in the paperboard for these two cases?

In the first setup, an initial velocity condition of 10 m/s is applied to the paperboard in the longitudinal direction. During the analysis, a velocity boundary condition is applied on the outflow surface to maintain the velocity of the paperboard. Thus, a constant flow of the paperboard is sought for in the analysis. From the simulation it is concluded that the velocity is held constant for this test.

In the setup, there are no forces or accelerations acting on the paperboard, why it should not contain any internal stresses. After viewing the von Mises stress in the paperboard it is however noticed that the material is not completely stress-free. The magnitude of the obtained stress is very small (1×10^{-14} MPa) and is considered negligible. Despite the small stress obtained it is concluded that it is possible to have a paperboard flow through the Eulerian domain at a constant rate without any significant disturbance.

The ramping of paperboard flow is considered interesting to analyze. In the two applications, the flow and rotations is ramped up. A setup where the flow is ramped up with a velocity boundary condition on the outlet, is created and analyzed. Here it is of interest to investigate how different rates of the ramping affect the response in the material. Thus, ramping of the paperboard velocity is performed for four different ramping rates; 2, 4, 10 and 100 ms. Figure 3.4a displays the velocity for the different ramping rates at RP1 while Figure 3.4b shows the von Mises stress responses.

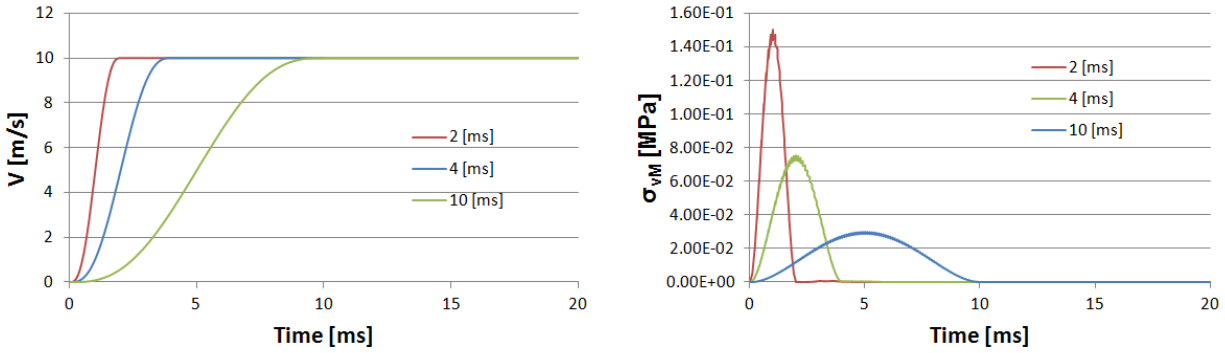

(a) Velocity

(b) von Mises stress

Figure 3.4: The response in RP1 when the velocity is ramped up over 2, 4 and 10 ms

The final velocity of 10 m/s is achieved for all ramping rates, including the 100 ms setup which is not displayed in Figure 3.4. It is clear that a faster ramping gives rise to a higher stress in the material, which is shown in Figures 3.4b. The highest von Mises stress from the 100 ms of ramping setup is approximately 3.0×10^{-3} MPa. The way that the ramping affects the material response is expected. Higher accelerations gives rise to larger material responses. Hence, there is always a trade off between the rate of the ramping and how high stresses in the material that are acceptable. There is not only one correct way to treat this trade off but it should be handled individually for each application.

3.1.2 Analysis of the effects on the paperboard due to stress conditions

In the web motion problem, the paperboard is under a tensile stress. Therefore it is interesting to see how it is possible to achieve a tensile stress in the paperboard for this problem. Initially a static problem is studied. It is investigated whether it is possible to introduce a tensile stress as an initial condition and then hold it constant with boundary conditions. The possibilities to ramp up a tensile stress is also studied.

A setup where a tensile stress is applied initially, and held constant throughout the analysis is tested. The analysis runs over 100 ms and due to the initial- and boundary conditions no changes in the paperboard should be detected. This is also how the material behaves. The von Mises stress in the paperboard is held constant throughout the analysis while no velocity is present in the paperboard.

In the web motion application, ramping of a tensile stress is important to achieve since this is a procedure in the production. Therefore, it is of interest to investigate the possibility to ramp up a tensile stress in the paperboard from a stress free initial state, why such a test is conducted. No velocity in the paperboard is included in the analysis. The tensile stress in the paperboard is ramped up during the analysis by locking the outlet surface with a zero velocity boundary condition, while a pressure load is ramped up on the inlet surface. Ramping rates of 2, 4, 10 and 100 ms are tested. The velocity and stress responses for these analyses are displayed in Figures 3.5 and 3.6.

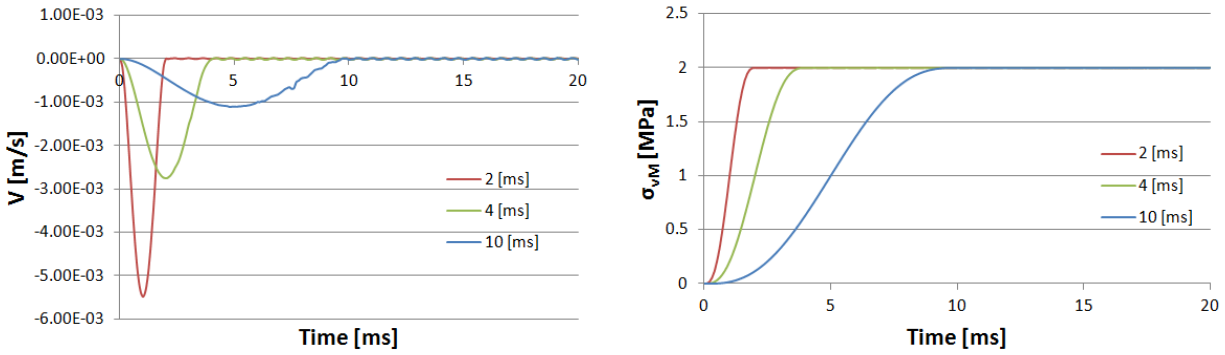

(a) Velocity *(b) von Mises stress*

Figure 3.5: Velocity and stress response in RP1 when the tension is ramped up over 2, 4 and 10 ms

By looking at Figure 3.5b it is clear that the desired tension of 2 MPa is achieved for 2, 4 and 10 ms of ramping. The fact that a faster ramping leads to a greater material response is again seen in Figure 3.5a. From Figure 3.5a it may also be noted that small oscillations of the velocity start to occur by the end of the ramping, which continues throughout the rest of the analysis. It is possible to hold a constant tension in the paperboard according to the previous test, where a stress initial condition was applied and then held constant. The dynamic effects when ramping the tension in the paperboard must therefore affect the analysis. Interestingly, a slower rate of ramping seems to lead to higher oscillations. This is seen in Figure 3.6, where the ramping is performed over 100 ms. Large oscillations on the velocity is seen, and even oscillations on the von Mises stress are visible.

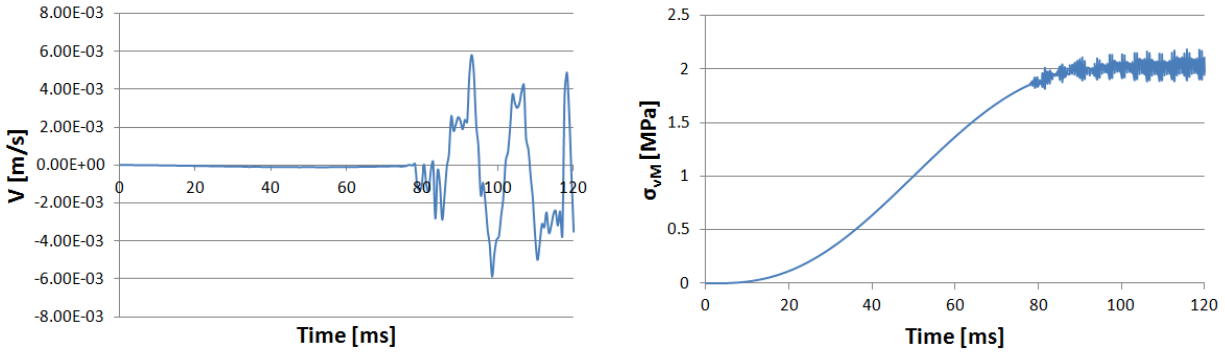

(a) Velocity *(b) von Mises stress*

Figure 3.6: Velocity and stress response in RP1 when the tension is ramped up in 100 ms. Oscillations start to occur after approximately 75 ms

The behavior displayed in Figure 3.6 contradicts the general idea of how the rate of ramping affects the material response. A slower ramping should lead to less disturbance due to smaller accelerations of the nodes, but here the disturbance is significantly higher compared to the previous simulations where higher rates of ramping are used. The identified oscillations in the paperboard thus seem to increase when the rate of ramping is decreased. One possible reason for this behavior might be due to instabilities.

3.1.3 Analysis of the effects on the paperboard due to combinations of velocity and stress conditions

In the web motion problem, a tensile stress and a flow of the paperboard are present, why such tests are conducted. In the first setup, two initial conditions are applied; a predefined tensile stress and a flow of paperboard. Thereafter, the tensile stress and paperboard flow are held constant with the applied boundary conditions. In the second setup, a velocity initial condition is applied while the stress is ramped up. In the third setup, a stress initial condition is applied while the velocity of the paperboard is ramped up. The ramping times used for these test are 2, 4 and 10 ms.

In the first setup, a predefined tensile stress of 2 MPa and a predefined velocity of 10 m/s are applied. The stress and velocity are then held constant with two boundary conditions on the inlet and outlet surfaces. Figure 3.7 displays the stress and velocity response for this setup.

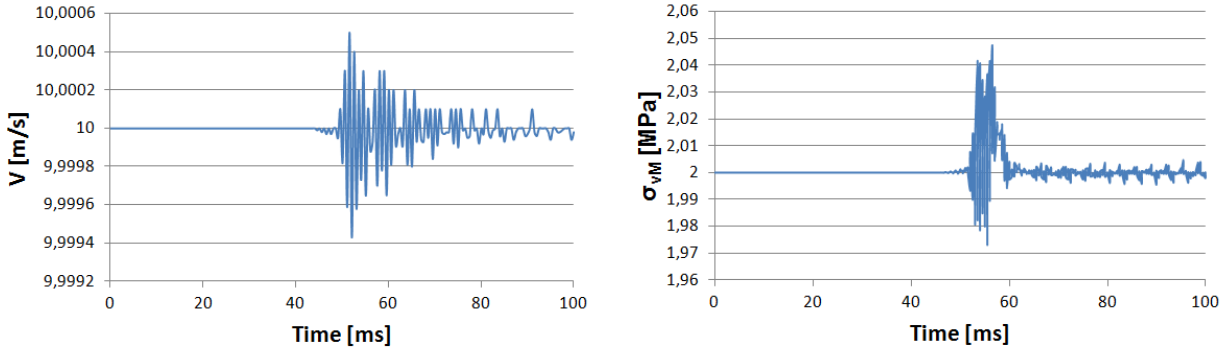

(a) Velocity *(b) von Mises stress*

Figure 3.7: Velocity and stress response on RP1 when the velocity and tension is held constant. Oscillations starts at approximately 50 ms

Initially, the stress and velocity on RP1 are constant, as expected. However, after circa 50 ms some oscillations in the paperboard starts to occur. The von Mises stress is increased by approximately 2.5% at most and the velocity by 0.004% at most. These oscillations are not expected in this analysis. Some instabilities in the analysis are seen.

A small investigation of how the time increment affects the analysis is performed. The time increment is normally obtained through the Abaqus/Explicit default setting and is recalculated for each increment. The time increment is found to be approximately 5.722×10^{-5} ms during the whole analysis why this is used as the standard time increment. In one test, the time increment is increased with 50% while in an other test the time increment is decreased with 50%. What is first discovered is that the test where an increased time increment is used, is not applicable. When the time increment is increased, the deformation speed to wave speed is too large (over 1.0). This means that some material in the analysis may deform to such extent in a time increment that it will completely skip one whole element in the increment, which is prohibited. Thus, no solution is obtained. When running the same simulation with smaller time increment, the same behavior can be seen. The difference is that the oscillation is delayed by approximately 15 ms.

In the next setup the tension is ramped up while a constant flow of paperboard is prescribed and held constant throughout the analysis. Figure 3.8 illustrates the result from this analysis where 2, 4 and 10 ms of ramping are tested. Another setup is obtained prescribing the tension and holding it constant while the velocity is ramped up. The same ramping speeds are used as for the previous test. Figure 3.9 displays the result from this analysis.

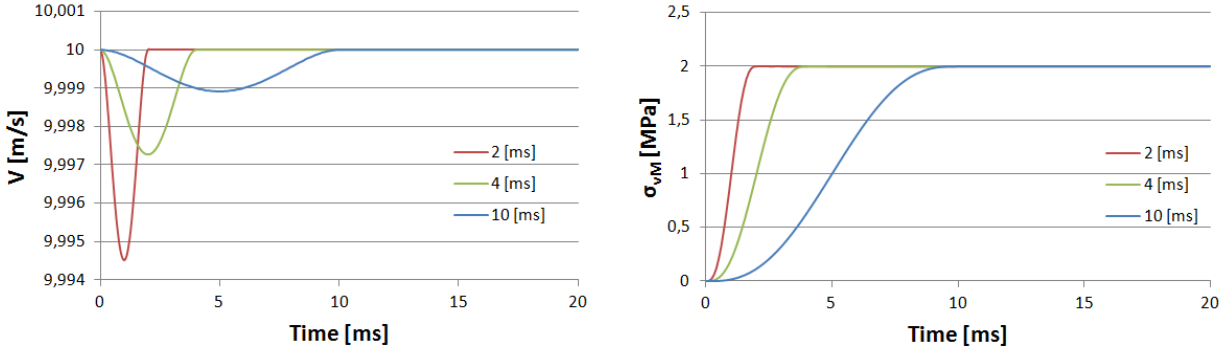

(a) Velocity *(b) von Mises stress*

Figure 3.8: Velocity and stress response at RP1 when the velocity is held constant while the tension is ramped up over 2, 4 and 10 ms

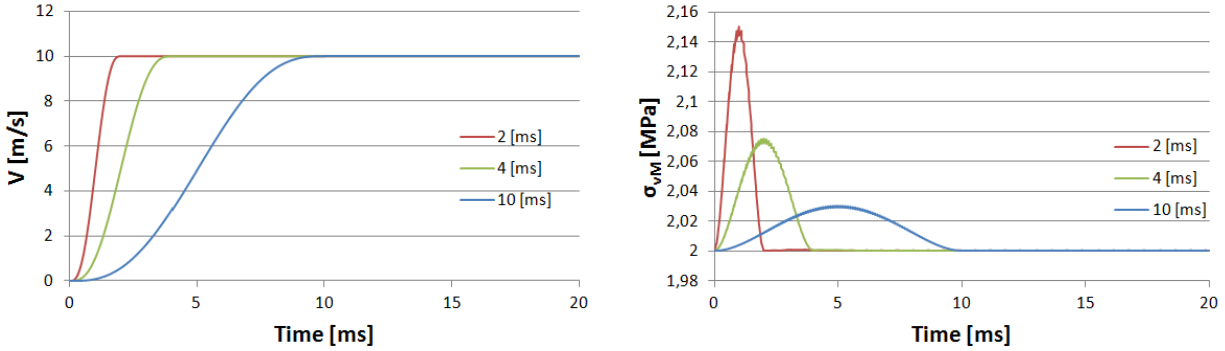

(a) Velocity. *(b) von Mises stress*

Figure 3.9: Velocity and stress response on RP1 when the velocity is ramped up while the tension is held constant

It is noticed that by ramping up the tension while a velocity is present, or ramping up a velocity while a tension is present, gives the expected result. The results from these analyses show no oscillation that has been seen in some of the previous simulations. However, if comparing the analyses with the one displayed in Figure 3.7, it is noticed that the latter one has a longer simulation time and that the oscillations initiates late in the analysis.

3.1.4 Analysis of the coupled Eulerian-Lagrangian contact

It is of great importance that the contact between the nip- and chill roller, as well as the contact between the paperboard and the rollers, are modeled accurately. A contact test is created for the plate. In the setup, a steel plate is created using the Lagrangian approach. The material model is isotropic with Poisson's ratio of 0.3, a density of 7.356×10^{-3} g/mm^3 and the Young's modulus of 2.1×10^5 MPa.

Figure 3.10 displays the two setups that are investigated. The objective with the test is to study how the obtained coupled Eulerian-Lagrangian contact pressure is affected by the position of the paperboard within the Eulerian domain. That is, how will the contact pressure differ if the paperboard surface is within an element filled with paperboard till 100%, compared to the contact pressure obtained if the paperboard surface is within an element filled till less than 100% paperboard.

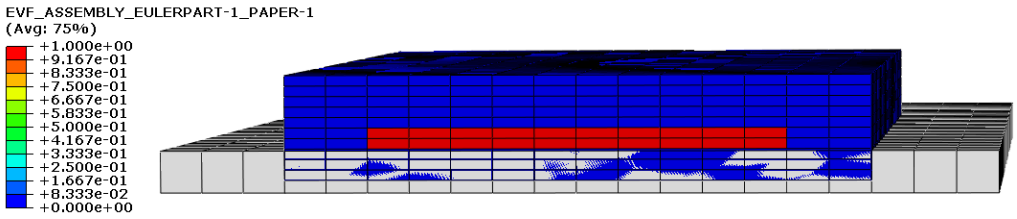

(a) The paperboard position is adjusted to fit the Eulerian mesh so 100% filled elements are achieved

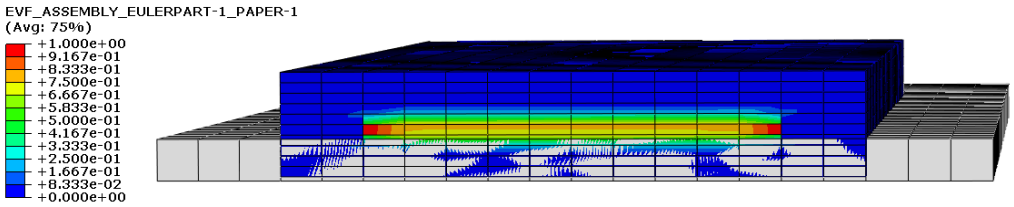

(b) The paperboard position is not adjusted to fit the Eulerian mesh so less than 100% filled elements are achieved

Figure 3.10: Two initial setups for investigation of contact pressure. The dimensions of the paperboard are the same. In (a) the paperboard is fitted exactly into two Eulerian element thicknesses and in (b) the paperboard is fitted randomly in the Eulerian domain

The paperboard is subjected to an arbitrarily chosen body force of 1 N/mm^3 in the direction towards the steel plate. The paperboard is thus pushed on the steel plate and a contact pressure on the steel plate is obtained. The body force is ramped over 20 ms and then the load is held constant for an additional 10 ms. Figure 3.11 illustrates the contact pressures on the steel plate for the two different configurations.

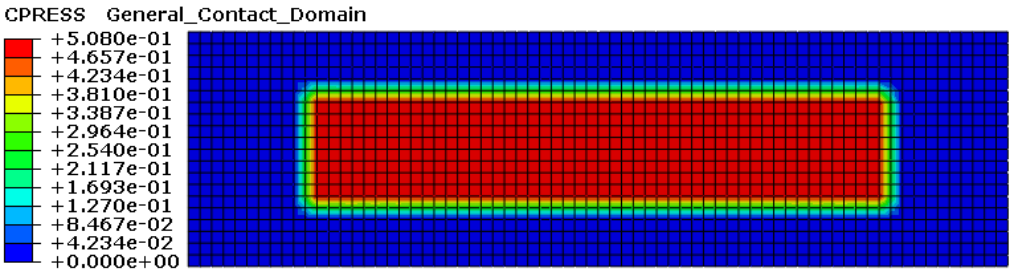

(a) The paperboard is placed to fit the Eulerian mesh

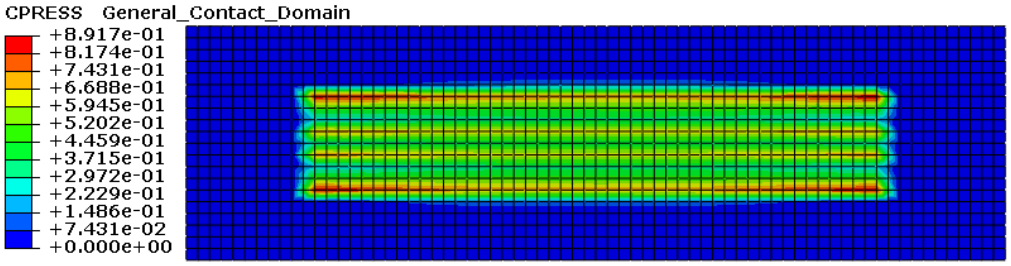

(b) The paperboard is not placed to fit the Eulerian mesh

Figure 3.11: Contact pressure MPa on the plate when the paperboard is pushed against the plate. Different placements of the paperboard within the Eulerian domain are showed

It can be seen that the obtained contact pressure becomes more accurate if the paperboard surface lies within an element filled till 100% paperboard. This is according to *Abaqus Analysis User's Guide* (2014) and needs to be taken into account.

3.1.5 Effects on the run time due to changes of the model and element sizes

To understand how the simulation time is affected by a change of either the model size or of the element size, a couple of tests are performed. The static setup seen in section 3.1.2 is used. The first test is performed to study how different element sizes affect the run time. Aside from the standard element size, three additional element sizes are tested. The same aspect ratio used for the standard element size, is used for the three other element sizes. That is, the length and width of the elements are four times larger than the thickness of the element. The four different element sizes are chosen so there are two, four, six or eight elements in the paperboard thickness, and the width and length of the elements are chosen according to the aspect ratio. Table 3.2 displays the result from this test.

Table 3.2: How the change of element size affects the run time. Element dimension displayed in thickness×length×width

Element dimension [mm]	$0.25 \times 1 \times 1$	$0.125 \times 0.5 \times 0.5$	$0.0833 \times 0.333 \times 0.333$	$0.0625 \times 0.25 \times 0.25$
Paper size [mm]	$0.5 \times 50 \times 10$	$0.5 \times 50 \times 10$	$0.5 \times 50 \times 10$	$0.5 \times 50 \times 10$
Number of elements	7000	56000	189000	448000
Number of nodes	8415	61509	201283	469737
Run time [s]	154	1924	9106	23019
Smallest time increment [ms]	5.7×10^{-5}	2.9×10^{-5}	1.9×10^{-5}	1.4×10^{-5}

The decrease of element size leads to an increase of the number of elements and decrease of the smallest time increment. Therefore, the analysis is prolonged both due to the smaller time increment and due to the increased number of elements.

In the second test, the element size is held constant while the width of the paperboard is increased. Table 3.3

displays the results from these tests.

Table 3.3: How the change of model size affects the run time

Element dimension [mm]	$0.25 \times 1 \times 1$	$0.25 \times 1 \times 1$	$0.25 \times 1 \times 1$	$0.25 \times 1 \times 1$
Paper size [mm]	$0.5 \times 50 \times 10$	$0.5 \times 50 \times 50$	$0.5 \times 50 \times 100$	$0.5 \times 50 \times 500$
Number of elements	7000	27000	52000	252000
Number of nodes	8415	30855	58905	283305
Run time [s]	154	477	1077	4336
Smallest time increment [ms]	5.7×10^{-5}	5.7×10^{-5}	5.7×10^{-5}	5.7×10^{-5}

It is noticed that the time increment is constant for all setups since the element dimensions are held constant. Thus, only the variation of the number of elements results in an increased run time.

Figure 3.12 displays the simulation time for the two tests versus the number of nodes in the models. An almost linear behavior is displayed. It is seen that changing the element size affects the runtime more than changing the model size. This is because a change of the model size affects both the number of elements and the time increments in the solution.

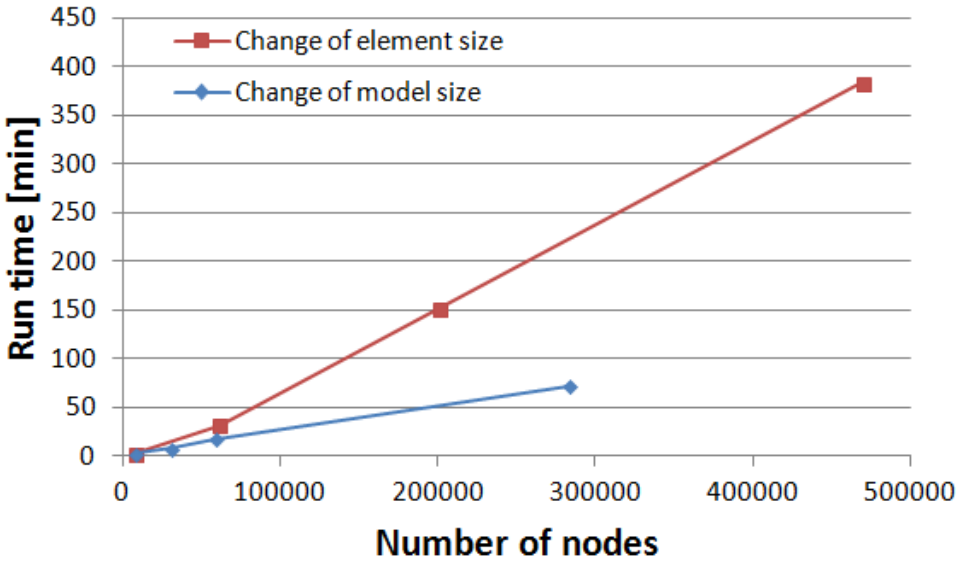

Figure 3.12: Results from the analyses when the width of the model is changed while the element size is held constant, and when the size of the elements are changed while the size of the model is held constant

3.2 Conclusions from the investigation of Eulerian modeling in Abaqus

The Eulerian modeling technique displays the functionality necessary to proceed with the method. The Eulerian boundary conditions, where material freely can flow in and out of the Eulerian domain, works according to theory. However, some numerical difficulties were detected for some of the analyses made. This might be something that need to be addressed in further analyses. There might be some difficulties to obtain the velocities and tension in the models. Furthermore, the contact problem is very important for both the web motion and the nip problem. Either the mesh needs to be fine in the contact regions or the material assignment in the Eulerian domain needs to be performed with precision.

4 Web motion analysis

In this chapter the web motion problem will be analyzed. First a general description of the model parameters will be given together with the model validation parameters. Next, the Eulerian method will be presented followed by the periodic media analysis.

The paperboard and the steel are for simplicity given isotropic linear elastic material properties. The properties are shown in Table 4.1.

Table 4.1: Material properties used in the model. Pb is short for paperboard while S is short for steel

Properties		
ρ_{pb}	6.56×10^{-4}	[g/mm^3]
E_{pb}	9000	[MPa]
ν_{pb}	0.2	
ρ_s	7.356×10^{-3}	[g/mm^3]
E_s	210 000	[MPa]
ν_s	0.3	

In the models, the paperboard should have a velocity of 10 m/s.

To validate the accuracy of the models used for web motion a couple of validation criteria are used. The first is the tension in the paperboard. At the production cite, the paperboard is stretched with a load corresponding to 1 N/mm paperboard width. Thus, the force exerted on a paperboard of width w, through the cross direction is $1 \times w$ N. The cross section area of a paperboard with 0.5 mm thickness and width w is $0.5 \times w$ mm^2. Thus, a tensile stress of 2 MPa is present in the paperboard according to $\sigma = \frac{F}{A} = \frac{1.0 \times w[N]}{0.5 \times w[mm^2]} = 2$ MPa, where F is the force and A is the cross section area.

The contact pressure is given by Vedmar (1998) as:

$$p = \frac{T - \rho h w R^2 \Omega^2}{wR} \tag{4.1}$$

where T is the pretension force corresponding to 1 N/mm, ρ the density, Ω the rotational velocity, h the thickness of the paperboard, R the radius of the roller and w the width of the paperboard.

The contact pressure obtained is 0.01 MPa which will be used as a reference for the contact pressure between the rollers and the paperboard in the following models.

4.1 Web motion using the coupled Eulerian-Lagrangian method

A web motion problem is constructed using the coupled Eulerian-Lagrangian method. Initially a simplified setup is used and evaluated to see what further actions that can be taken. This model is very thin and contains of one roller and one short piece of paperboard that covers 180° of the roller. The model is tested and validated by the following chosen data obtained from the simulations; contact pressure between the paperboard and the roller, stresses in the paperboard and velocity or movement of the paperboard.

4.1.1 Model description of thin model with one roller

The model is displayed in Figure 4.1. The roller has an outer diameter of 200 mm, a width of 7 mm and the thickness of 1 mm. The material properties listed in Table 4.1 are used. The roller is meshed using linear hexahedral, reduced integration, eight node 3D deformable elements (C3D8R in Abaqus). The element size is 1.0×1.0×1.0 mm leading to a total number of 5024 elements for the whole roller.

The Eulerian domain is the part colored blue in Figure 4.1. It has the same shape as the paperboard it contains, but is wider and thicker. The thickness is 2.5 mm and the width is 7 mm. The straight ends are 50 mm long each and the curved part follow the cylinder's curvature. The inner diameter of the Eulerian domain's curvature is 198.5 mm, so the Eulerian domain and the roller overlaps to make the coupled Eulerian-Lagrangian contact. The paperboard is placed tight onto the cylinder. It is assigned its position in the Eulerian domain through the creation of a paper set which is filled with paperboard. With this approach, the elements containing paperboard is 100% filled with the material. The paperboard is assigned a width of 3 mm and a thickness of 0.5 mm.

The chosen Eulerian element type is the same as for the flat paperboard model, EC3D8R in the Abaqus. The standard element dimensions are set to 0.25×1.0×1.0 mm through the thickness, length and width respectively. The meshing is obtained so that the elements follow the curvature, thus the material assignment becomes as good as possible. The meshing is performed for the best possible contact between the paperboard and the roller where the result from the flat piece of paperboard is taken into account.

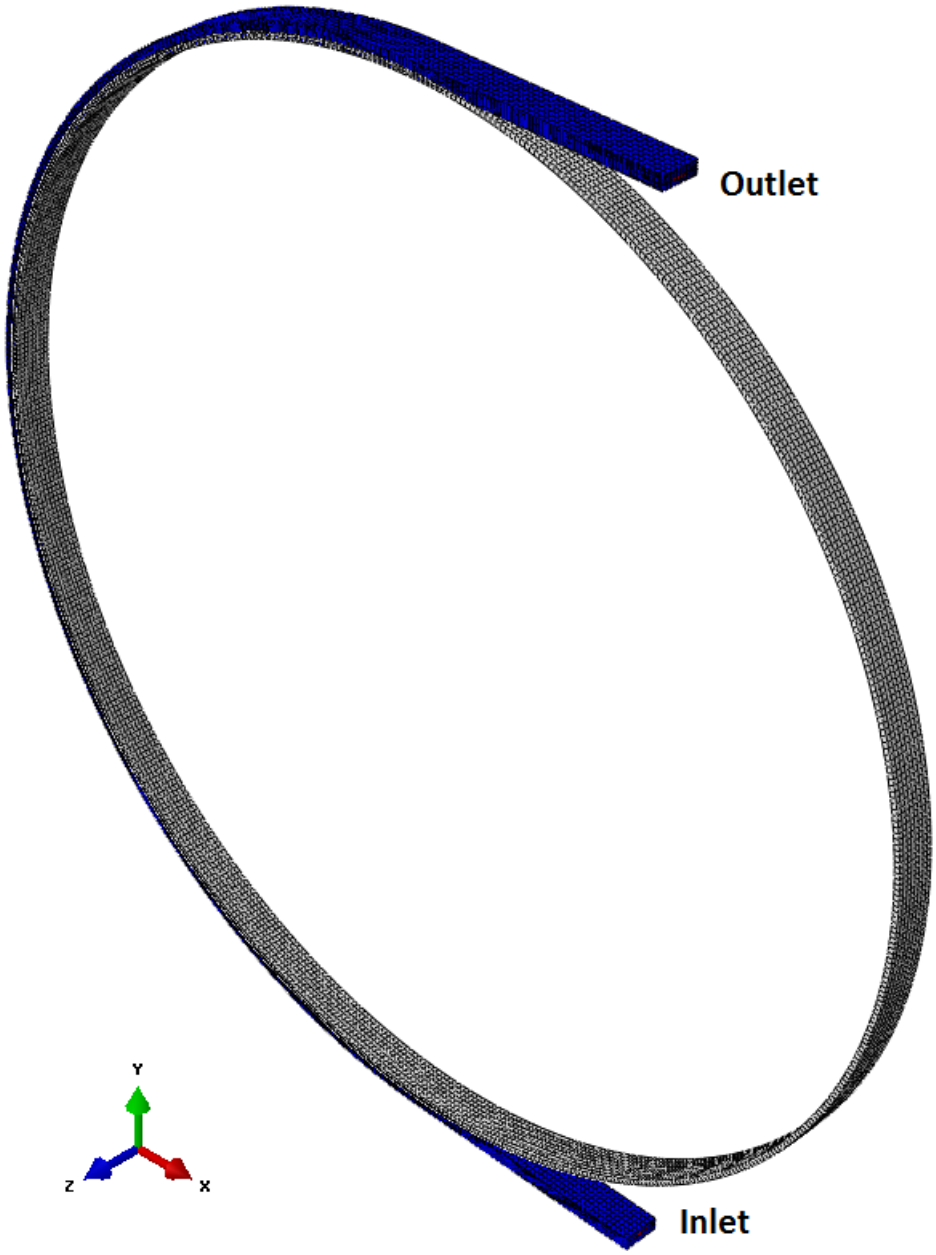

Figure 4.1: The thin Eulerian model with one roller

Figure 4.2 shows the model in more detail, Figures 4.2a-4.2c display a cross section of the model from different views. In the figures, the material assignment of paperboard in the Eulerian domain is visible. The material assignment is made so that an element is either completely filled with paperboard (the red elements in figures) or completely filled with void (blue elements in the figures). In Figure 4.2c it can be see that the element is placed directly upon the roller so that there is no gap between the two when the analysis begin. Figure 4.2d displays the paperboard position of the paperboard viewed from the outlet surface of the model. From this view it is noticeable that the paperboard is allowed to move in the cross direction (z-axis) and in the thickness direction of the paperboard.

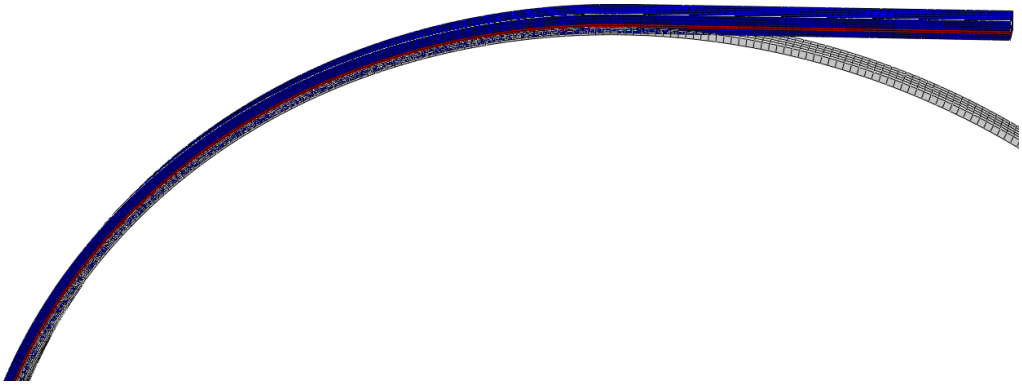

(a) Upper part of the model, called the outlet

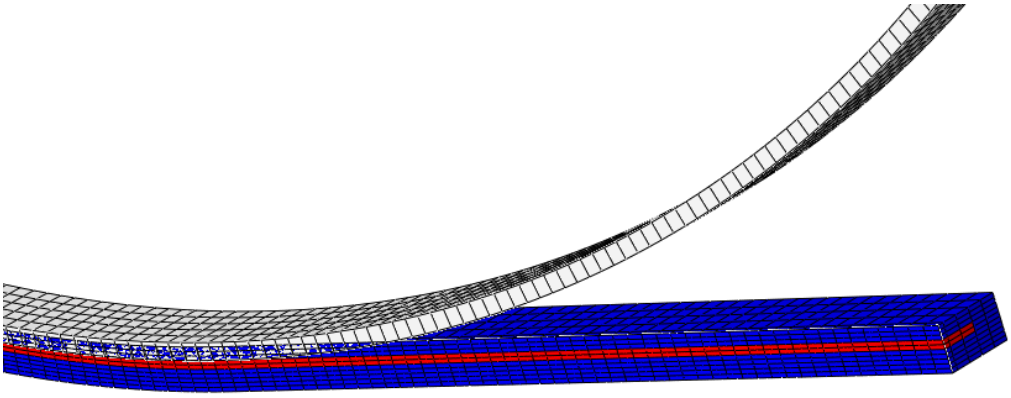

(b) Lower part of the model, called the inlet

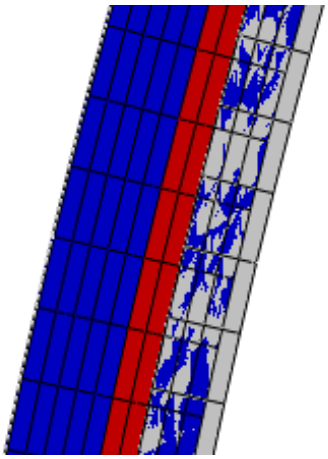

(c) A cross-section cut of the initial setup and position of the paperboard in relation to the roller

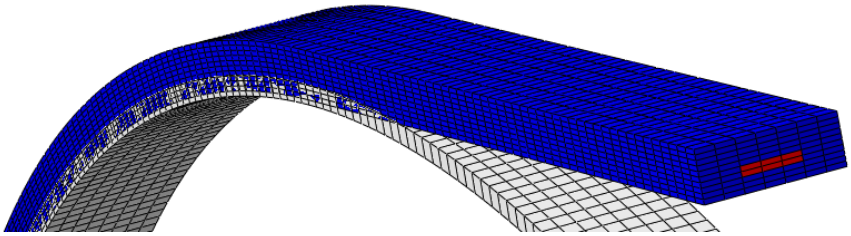

(d) Figure of the outlet where the red elements represent the paperboard

Figure 4.2: The Eulerian model illustrated from different views

To measure the contact pressure, a path on the roller consisting of element nodes is created, see Figure 4.3.

The path is in the machine direction (along the length of the paperboard) and it covers the whole length where the contact between the paperboard and roller occurs. It is positioned in the middle of the paperboard in the cross direction.

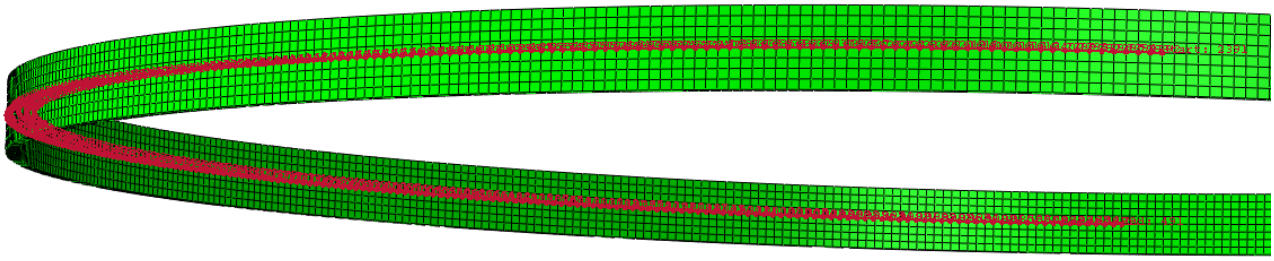

Figure 4.3: The path on the roller from where the contact pressure is measured

The collected stresses from the simulation are obtained from three different positions in the paperboard. Figure 4.4 shows the positions and nodes where the stresses are investigated. The nodes chosen lie in the middle of the paperboard in the cross section.

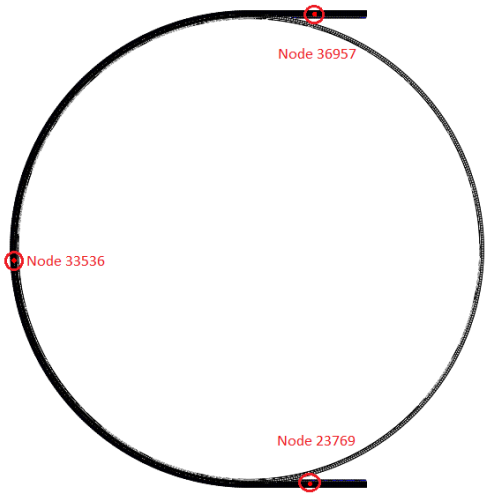

Figure 4.4: The nodes in the Eulerian domain from where σ_{vM} is measured

Boundary conditions, initial condition and interaction properties

The roller is subjected to two different boundary conditions. Either the roller is fixed in space throughout the entire analysis, or the roller is moved to create tension in the paperboard and then fixed in space afterwards. When the roller is moved, it is strictly in the negative x-direction and thus a tensile stress is induced in the paperboard. The displacement is iteratively determined to 0.23 mm which gives a von Mises stress of 2 MPa in the paperboard after the displacement. To allow some deformation on the outer surface of the roller, it is the inner surface that the displacement boundary conditions are applied to.

There are two Eulerian boundary conditions in the model. They are applied at the inlet and outlet of the Eulerian domain and the paperboard. The boundary condition applied to the inflow surface is a free inflow of paperboard and the boundary condition applied to the outflow surface is a free outflow of paperboard. Thus, new paperboard flowing in from the inflow surface is allowed while the paperboard flowing out of the outflow surface can do so without any prevention.

The inlet surface is subjected to two additional boundary conditions. A negative pressure load of 2 MPa may be applied to the surface. This pressure load is to either ramp up the tension in the paperboard or to hold a

constant tension in the paperboard. A velocity boundary condition may also be applied to the inlet surface. This velocity is used to either fix the paperboard by using a zero velocity condition, to ramp up the velocity in the paperboard or to hold a constant velocity of 10 m/s in the paperboard. The same velocity boundary conditions are applied to the outlet surface.

A velocity initial condition may be applied to the paperboard in some setups. The velocity is then set to 10 m/s in the machine direction and is then held constant through the velocity boundary conditions on the inlet and outlet surfaces.

For the coupled Eulerian-Lagrangian contact the default settings in Abaqus are used. In the normal direction, the pressure-overclosure is chosen to be that of "Hard" Contact and the constraint enforcement method used is the penalty method. In the tangential direction, the contact between the paperboard and roller is chosen to be frictionless. Thus, paperboard will be able to flow over the roller that has a fixed rotation velocity.

4.1.2 Test of static setup - achieving a tensile stress in paperboard without any flow of paperboard

A static test is conducted to investigate whether it is possible to obtain a desired tensile stress in the paperboard and to obtain a desired contact pressure over the roller. Two different setups are used in this test. In the first setup, the outlet is fixed due to a zero velocity boundary condition while the inlet surface is subjected to a negative pressure load of 2 MPa, which is ramped with different rates. The roller is fixed by the zero displacement boundary condition. In the second setup the inlet and outlet are fixed with the zero velocity boundary condition while the cylinder is moved 0.23 mm in the negative x-direction.

A contact pressure on the roller of 0.01 MPa and a stress in the paperboard of 2 MPa are desired in the simulations. Figures 4.6 and 4.5 show the von Mises stresses at the three nodes and the contact pressure over the path for the two different setups. In Figure 4.5, the stress in the material is achieved through ramping up the pressure load over 10 ms. In Figure 4.6, the stress in the paperboard is achieved by increasing the roller displacement during 4 ms.

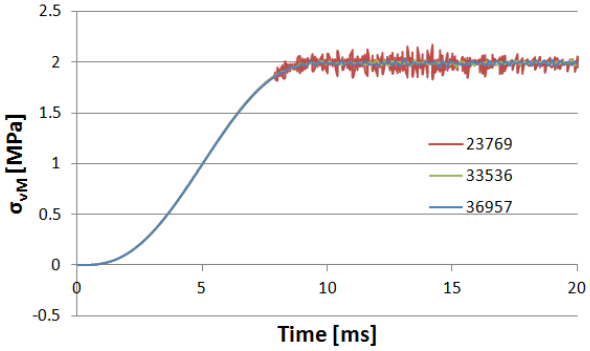

(a) σ_{vM} on the three selected nodes

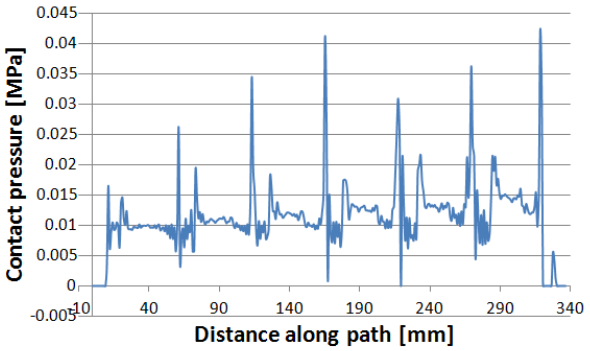

(b) Contact pressure over the path

Figure 4.5: Result from the simulation when the tension in the paperboard is achieved by ramping up a pressure in 10 ms

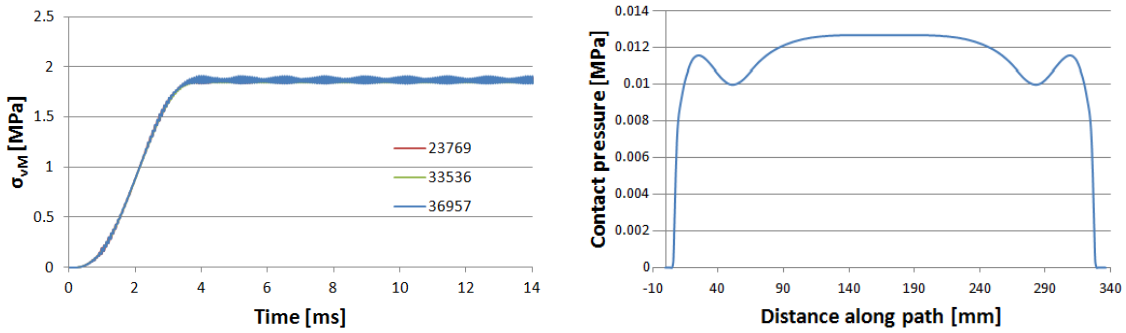

(a) σ_{vM} on the three selected nodes *(b) Contact pressure over the path*

Figure 4.6: Result from the simulation when the tension in the paperboard is achieved by moving the roller. The displacement is ramped in 4 ms

The achieved von Mises stresses for both setups, displayed in Figures 4.5a and 4.6a are stable but some oscillations do occur. The stress in the setup where the roller is moved is low, which is addressed later. The contact pressure over the path is displayed in Figures 4.5b and 4.6b. Here, the displacement of the cylinder setup gives a more continuous result compared to the second setup. Compared to the analytical contact pressure of 0.01 MPa the contact pressure is somewhat overestimated. Since the contact pressure is considered important, and the displacement controlled approach shows better results, this approach is chosen for further testing.

Figure 4.7a displays the volume fraction paperboard after the test where the cylinder is displaced. A volume fraction less than 100% is seen and the paperboard is spread out over a larger thickness than 0.5 mm. This will affect the output from the analysis. For example, the stress in the paperboard will be underestimated. Therefore, an additional setup is made where the element thickness is decreased. The element thickness is set to 0.125 mm and thus there are four elements through the thickness of the paperboard.

Figure 4.7 shows the volume fraction paperboard in the middle of the bend for the two setups when the roller has been displaced. In Figure 4.7a the element thickness is 0.25 mm while in Figure 4.7b the thickness is 0.125 mm. Here it is clear that the element thickness of 0.25 mm will not give accurate output since the volume fraction paperboard is less than 100%. For the other setup, where 0.125 mm thick elements are used, the volume fraction paperboard is 100% even over the bend, which gives the possibility of accurate data from the analysis, as concluded from the Eulerian analysis on the flat plate.

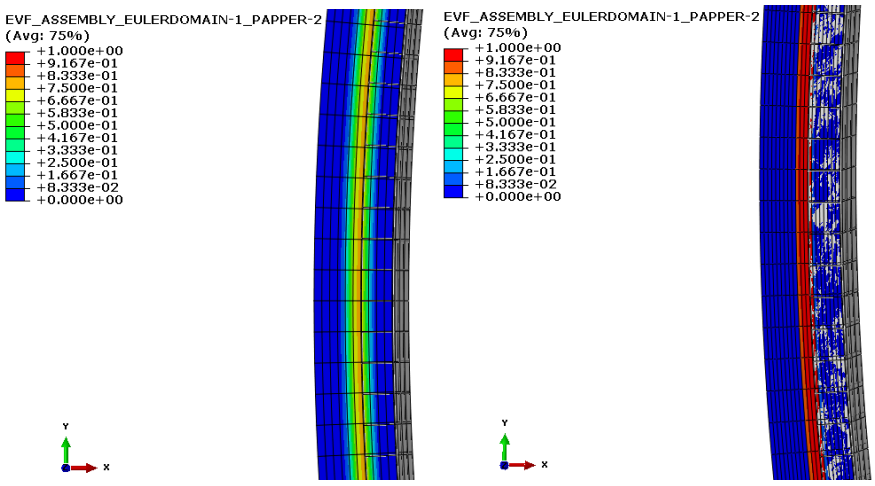

(a) Element thickness 0.25 mm *(b) Element thickness 0.125 mm*

Figure 4.7: Volume fraction of paperboard over the bend, after roller has been displaced

Figure 4.8 illustrates the obtained von Mises stress and contact pressure along the chosen path for the 0.125 mm element thickness setup. The stresses are measured in reference nodes at position similar to the ones used in the previous model. Nodes 42662, 62969 and 70721 in Figure 4.8a correspond to nodes in the upper straight part, in the middle of the bend and in the lower straight part of the Eulerian domain, respectively.

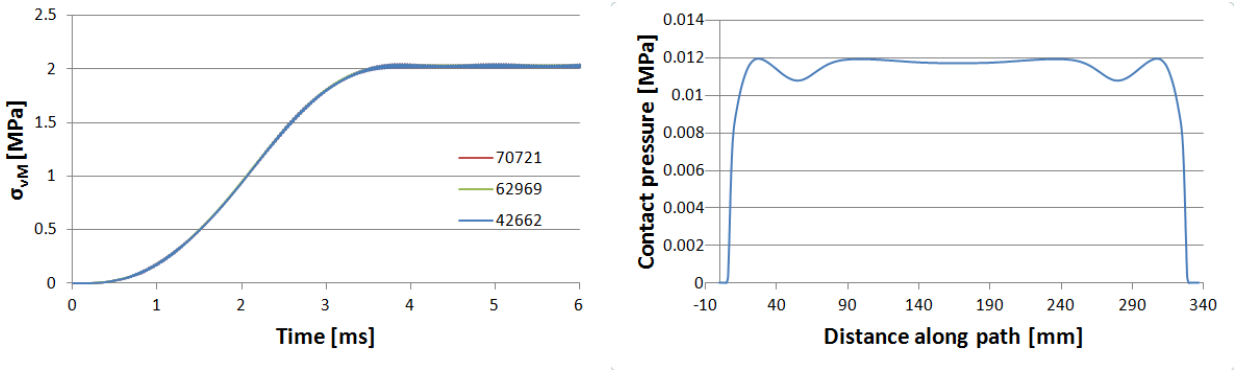

(a) von Mises stress at the three selected nodes *(b) Contact pressure over the path*

Figure 4.8: Results when a finer element thickness is reduced to 0.125 mm

In Figure 4.8a it is noticed that the von Mises stress in the paperboard is higher compared to the stress measured in Figure 4.6a. It is also noticeable that the fluctuation of the stress is decreased for the thinner element model. The contact pressure along the path is displayed in Figure 4.8b. The contact pressure behaves in the same way as in Figure 4.6b. It may however be noticed that the difference in contact pressure over the path is reduced compared to the contact pressure prestented in Figure 4.6b.

The tests performed show that the best way to achieve tension in the paperboard, when a realistic contact pressure between the paperboard and the roller is a key aspect, is to displace the roller while fixing the paperboard in the inlet and outlet. It is also concluded that the element thickness needs to be 0.125 mm for the possibility to achieve accurate results.

4.1.3 Dynamic setup - achieving a tensile stress while a flow of paperboard occurs

Next, a dynamic setup is created when flow of paperboard is added to the simulations. This setup contains two steps; a static step, where the tensile stress is achieved by displacing the roller, then the flow of paperboard is ramped up using velocity boundary conditions on the inlet and outlet surfaces.

Ramping of tensile stress followed by ramping of velocity

In the setup, an initial step in the analysis is to move the roller to obtain the tensile stress in the paperboard. The displacement of the roller is ramped in 4 ms and held constant for an additional 2 ms before the second step initiates. In the second step, the velocity in the paperboard is ramped in 10 ms then it runs for an additional 10 ms. The ramping rates are arbitrarily chosen. The element thickness in this simulation is 0.125 mm. Figure 4.9 displays the von Mises stress at three different locations in the paperboard.

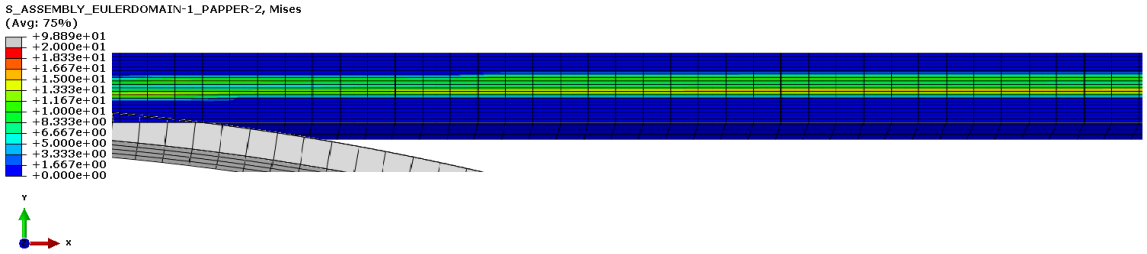

(a) Upper straight part, close to the outlet

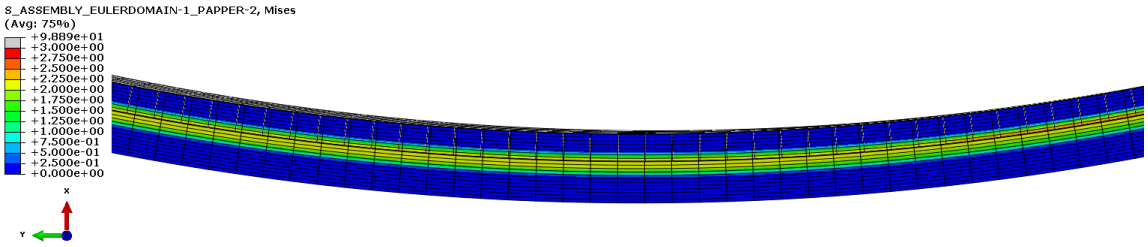

(b) Center part, over the bend

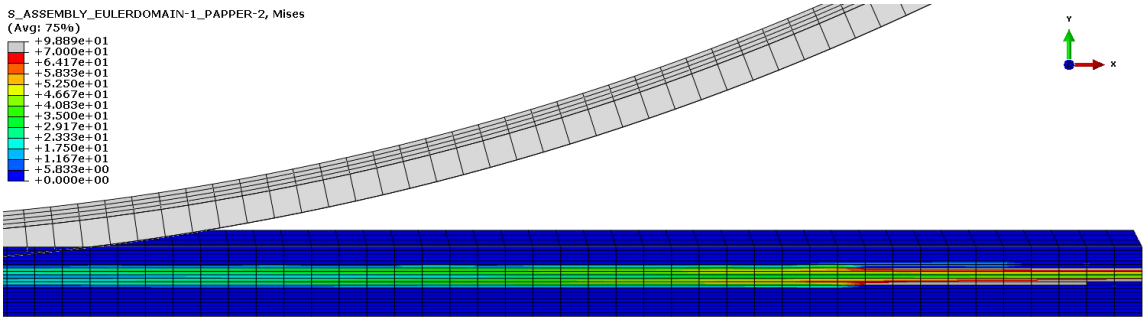

(c) Lower stright part, close to the inlet

Figure 4.9: σ_{vM} [MPa] for three different locations in the paperboard

In the upper straight part of the paperboard, Figure 4.9a, a higher von Mises stress is present in the material than the expected value of 2 MPa. This is also true for the lower straight part, prestented in Figure 4.9c, where the stresses in the paperboard are even higher. When looking at the von Mises stress at the paperboard which is in contact with the roller, Figure 4.9b the von Mises stress close to the expected value.

When looking at the obtained solution, oscillations of the paperboard on both the upper and lower straight part are visible. These oscillations may be the cause to the high stresses displayed in the material. Boundary conditions on the inlet and outlet surfaces constrain the movement of the paperboard in the thickness direction. These boundary conditions are necessary to prevent the paperboard from moving away, but they may contribute to the oscillations and high stresses obtained.

Figure 4.10 shows the contact pressure over the path on the roller. The magnitude of the contact pressure is the same as for the static test, see Figure 4.8b. However, the contact pressure fluctuates more, indicating that the dynamics of the system leads to a more inaccurate solution of the contact problem.

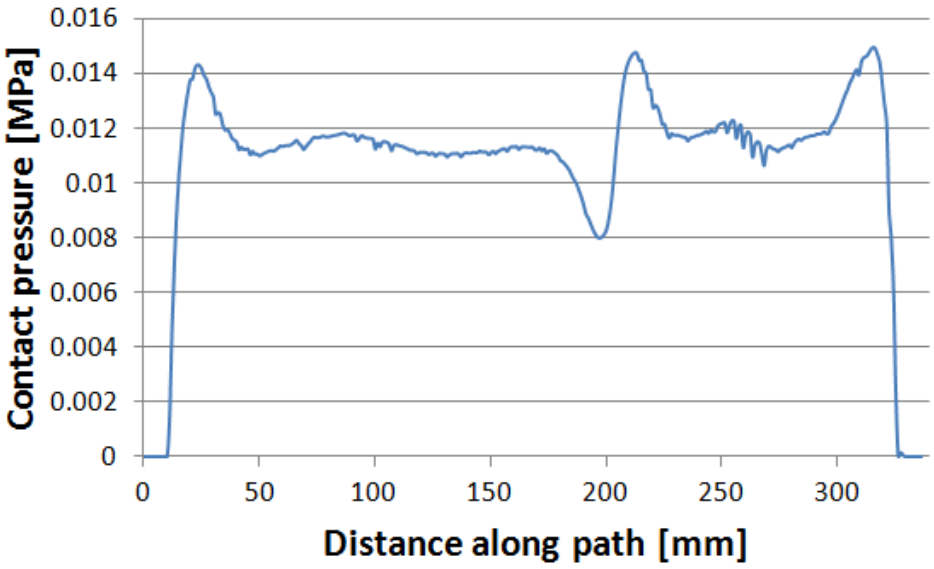

Figure 4.10: Contact pressure over the path for the dynamic test

It can be concluded that ramping a tensile stress in the paperboard while a constant flow of paperboard occurs is more problematic compared to ramping of the tension for a static setup. This somewhat contradicts what is seen on the Eulerian plate model. There, oscillations where seen when ramping a tensile stress on a static setup while it was not observed for a dynamic setup. However, in this setup, a coupled Eulerian-Lagrangian contact is present which increases the difficulty in the analysis. Another aspect that must be handled is that the run times of the simulations are long, which is covered in the following section.

4.1.4 Effects on run time of the Eulerian analysis in the web motion problem

A major issue regarding the coupled Eulerian-Lagrangian simulations is the run time. The analyses are computationally heavy and thus long run times are required. One reason for the long run times is the small time increment necessary for the analysis. The time increment is, as mentioned in the theoretical framework, dependent on the material data and the element size. The material data is given and constant, and the element size must be such that an accurate analysis is achieved. Therefore, there are no simple ways to increase the time increment to reduce the run time. To manually force a larger time increment than the default is not possible due to the fact that the ratio between the deformation speed to wave speed becomes too large resulting in a non-converging analysis. The magnitude of the time increment is 1×10^{-5} ms for these Eulerian simulations. With such time increment, the number of iterations will become large when performing simulations that in the end might need to be run over seconds. For example, if one second is to be run in the simulation, about 20 million time increments need to be performed in the analysis.

Also to keep in mind is that the current model is still simplified. The width of the paperboard is small, 3 mm. The model is also very short in machine direction, there is only room for one roller. The material model of the paperboard is linear elastic and isotropic. The roller is fixed in space and a zero friction interaction between the roller and paperboard is set. By changing the material properties, width of the model and the interaction properties between the paperboard and the roller will definitely increase the run time of the analyses.

An estimation of the run time based on the dynamic setup

The linearity between the width of a model and run time, displayed in Figure 3.12, is used to estimate how long run time a model in full width of 1500 mm would have. The setup tested is the dynamic one shown in the previous section. There, the width of the paperboard is 2 mm. A second analysis is done where the width of the paperboard is increased to 100 mm. When the run time for those two analyses are received, an estimation of the full width model can be made. For both the analyses, 24 CPU:s are used for comparability.

The element dimensions for the test is $0.125 \times 1.0 \times 1.0$ mm in length, width and thickness respectively and the simulation runs over 16 ms. The 3 mm setup contains of 63,824 elements and 82,032 nodes. The run time for the analysis was about 25 hours. The 100 mm setup consists of 938,912 elements and 1,060,185 nodes. The run time for the analysis became about 557 hours. By extrapolating these two values an estimation for a 1500 mm model is achieved. The estimated run time obtained is 8235 hours, or 340 days. This is considered infeasible with today's technology.

4.1.5 Discussion on Eulerian approach on web motion problem

The Eulerian modeling technique does not show any obvious advantages for modeling the web handling problem. It is difficult to achieve tension in, and flow of the paperboard. Further, it is hard to achieve an accurate contact since the paperboard surface is constantly estimated within the Eulerian domain. The Eulerian inflow and outflow allow the model length in the machine direction to be shortened but in terms of number of elements, the model size is not decreased. The paperboard dimensions are not very compatible with the Eulerian modeling. The thin paperboard require thin elements. Since the width of the paperboard and the length of the paperboard are so much larger than the width, this will lead to a large amount of elements.

Furthermore, the run time is to be considered infeasible. The main reason for this is the Eulerian mesh. The large amount of elements leads to long run times. The element dimensions also leads to small time increments, which in turn directly affect the run time. Due to the infeasible run times, it is decided that the Eulerian modeling of the web handling problem is not further studied in this thesis.

4.2 The periodic media analysis model

An alternative way of modeling the web motion is by using the Abaqus function called Periodic media analysis, see section 2.2.2 *Web Motion Modeled with Periodic Media Analysis*. To investigate this method, a simplified model on which the basic functionalities can be established is created initially. This model consists of a 100 mm wide piece of paperboard which moves with a predetermined tension in the paperboard. When the basic functionalities of the periodic media analysis is clarified, a larger model consisting of three rollers and the same size of paperboard is conducted. Finally, the paperboard in the model is widened to simulate the full size paperboard.

4.2.1 The paperboard model

To understand how the periodic media is implemented, a model consisting of a thin strip of paperboard is created. This model consists of 21 building blocks stacked vertically on each other, see Figure 4.11a. Each block is 100 mm long and 100 mm wide and the mesh size is ten by ten mm meaning that each block consists of 100 elements. The total length of the model is 2.1 m. The thickness of the blocks corresponds to the thickness of the paperboard and measures 0.5 mm. The element type used are shell elements and two different elements have been studied; the full integration shell element S4 and the reduced integration shell element S4R.

A display of the periodic media shuffling process, where a block is moved from the outlet to the inlet is seen in Figure 4.11b. To keep the boundary conditions at the outermost nodes, two specific nodes referred to as the inlet and outlet nodes are created and positioned arbitrarily. Figure 4.11b shows the positions of these nodes in this model. Figure 4.11b also illustrates the direction of the shuffling process of the building blocks and the defined trigger plane.

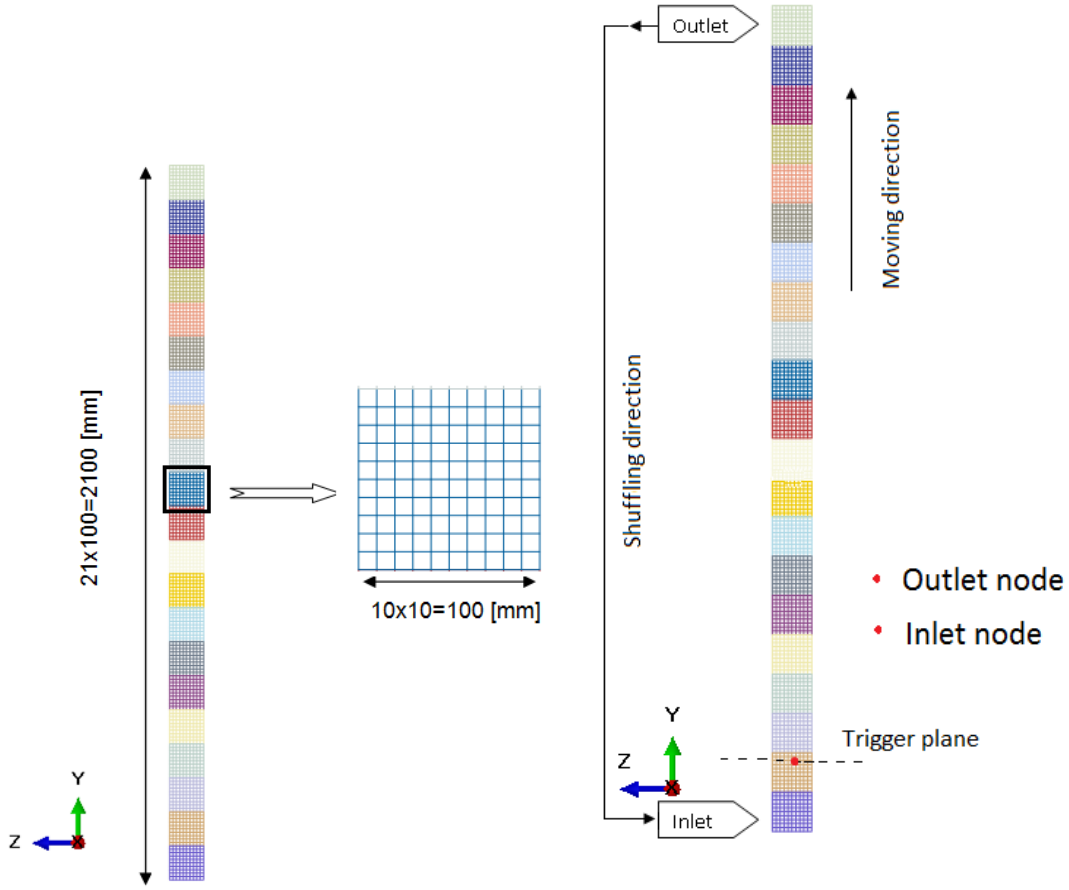

(a) The different colors represent the building blocks. On the right hand side, one building block is enlarged and the elements are displayed

(b) When the inlet block passes the trigger plane shuffling of the outlet block to the inlet takes place, the inlet and outlet nodes are presented

Figure 4.11: Description of the periodic media model

Initial conditions are used in the setup to reduce the run time and avoid ramping of the velocity. A uniform initial stress of 2 MPa is applied in machine direction, which here is the positive y-direction. An initial velocity of 10 m/s in machine direction is also added. The blocks are tied together with a node-to-node tie constraint defined in the periodic media function. The material used for the paperboard is isotropic and linear elastic with the same properties as the Eulerian model, see Table 3.1. In the analysis, the paperboard should continue to move with the initial conditions. To retain these conditions a concentrated load of 100 N is applied on the inlet node. A boundary condition of instantaneous velocity of ten meters per second is enforced on the outlet node. The applied initial conditions can be seen in figure 4.12 together with the boundary conditions and loads applied to maintain the velocity and stress through the paperboard.

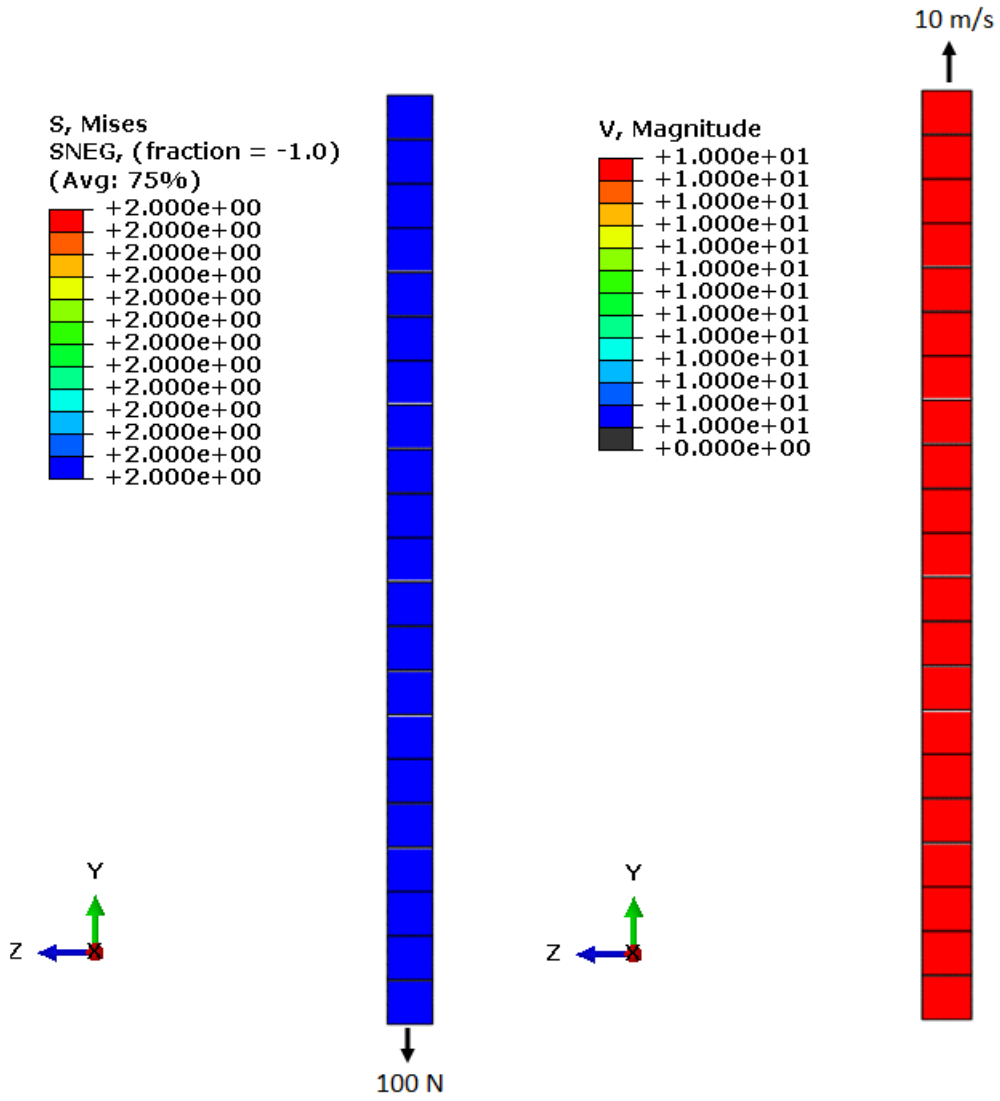

Figure 4.12: The left figure illustrates the pretension of 2 MPa and the applied load of 100 N needed to maintain the stress. The figure to the right illustrates the predefined velocity and the velocity boundary conditions of 10 m/s the outlet boundary to preserve the velocity. The velocities in x- and y-directions are set to zero

A small shock will appear when the shuffling occurs wherefore a small amount of mass proportional damping is recommended. The default material damping used in Abaqus is Rayleigh damping why it is used here. In this model the mass proportional damping, α, is set to 0.01 1/ms which is used for a similar problem in chapter [3.25] in the *Abaqus Verification Guide* (2014).

Two element types are tested in the analysis. One with full integration, the S4 element in Abaqus, and one with reduced integration, S4R. Reduced integration elements are known to be more simulation-efficient but they can suffer from hourglass effects. Full integration elements on the other hand do not have hourglass mode but can experience shear locking. Shear locking is a problem where shear stresses are introduced even though they do not exist. This is most common for quadrilateral elements such as the S4 element. When using reduced integration elements, different ways of hourglass control are available in Abaqus.

Importance of constraining the velocities at the inlet and outlet nodes

The upper edge on the inlet block is rigid, wherefore it is important that the same dimensions are kept through the inlet block. The rigid-body constraint is detected in Figure 4.13a where the deformation in the cross direction, here the z-direction, is scaled with a scaling factor of 1×10^6. A test was conducted to see the influence of constraining the inlet and outlet edges. If this is not done, the result will be as in Figure 4.13b where the simulation crashes after 191 ms due to excessive rotations. In this simulation, the edges are set free in the thickness(x)- and cross(z) directions. It can be seen that there are high stresses and large deformations where the edge is rigid, whereupon the simulation crashes. The reason for this might be the shock that arises when the blocks attach. This test illustrates the importance of constraining the velocity in these directions. Simulations where the velocities were constrained one by one were also performed with the same result shown in Figure 4.13. From here on the velocity at the inlet and outlet nodes, which are connected to the corresponding edges, is constrained to prevent warping. This approach also correlates with the procedure used in the Abaqus example on the periodic media analysis approach (*Abaqus Verification Guide* 2014).

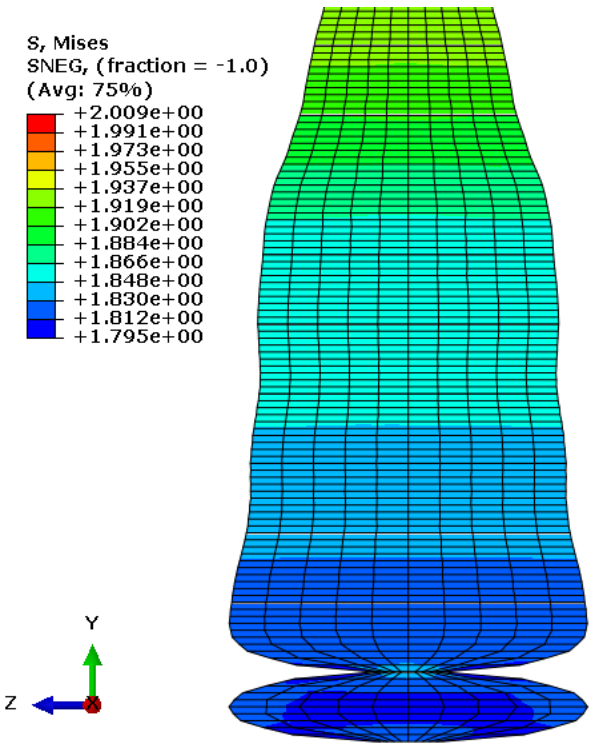

(a) The rigid body-like constraint at the front edge of the inlet block, the deformation in cross direction is scaled with a factor of $1 \cdot 10^6$

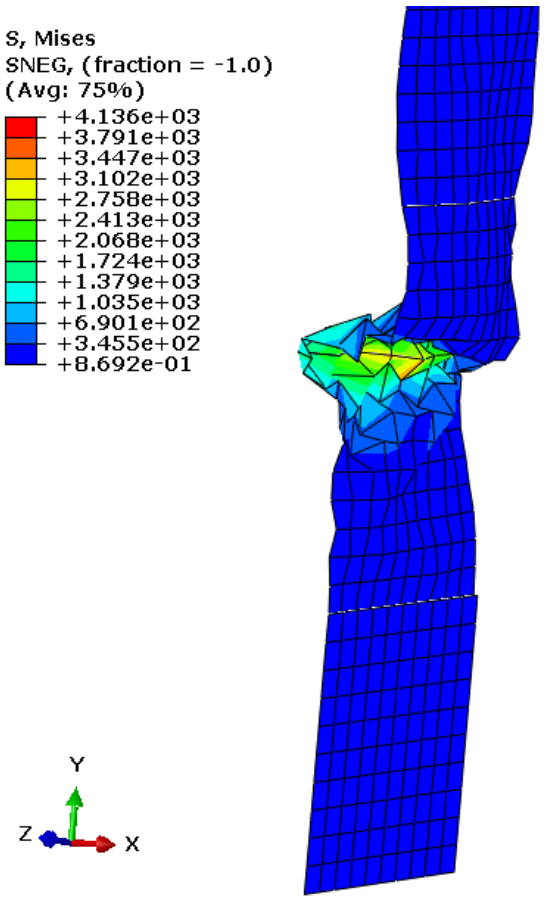

(b) After 191 ms, when the simulation crashes

Figure 4.13: Display of the importance of constraining the velocity in the direction where the periodic media should not move (the x- and z-directions). A close up display of the inlet section is seen in the figures

Stress distribution in the paperboard when using S4 elements

In this first simulation, the paperboard should move with a constant velocity of 10 m/s in machine direction with a retained stress of 2 MPa. The von Mises stress field after a three seconds simulation is seen in Figure 4.14.

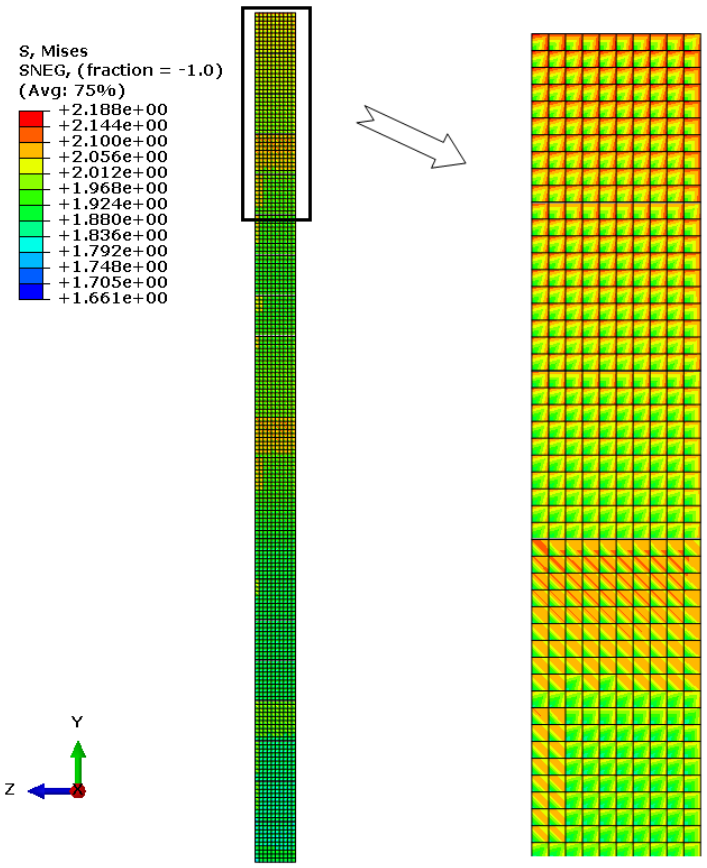

Figure 4.14: The von Mises stress in the paperboard after three seconds when S4 elements are used

A very unstable result is captured where the stress differs throughout the elements. One possible explanation to this phenomenon is shear locking. To avoid shear locking, reduced integration element are tested. Therefore, the next step is to create a model using S4R elements.

Stress distribution in the paperboard when using S4R elements

Since the fully integrated elements result in shear locking, reduced integration elements are used instead. Figure 4.15a shows the von Mises stress field after a three seconds simulation. The von Mises stress is similar to the stress in pure machine direction. A path is created in the middle of the paperboard along machine direction for which the normal stress is plotted, Figure 4.15b.

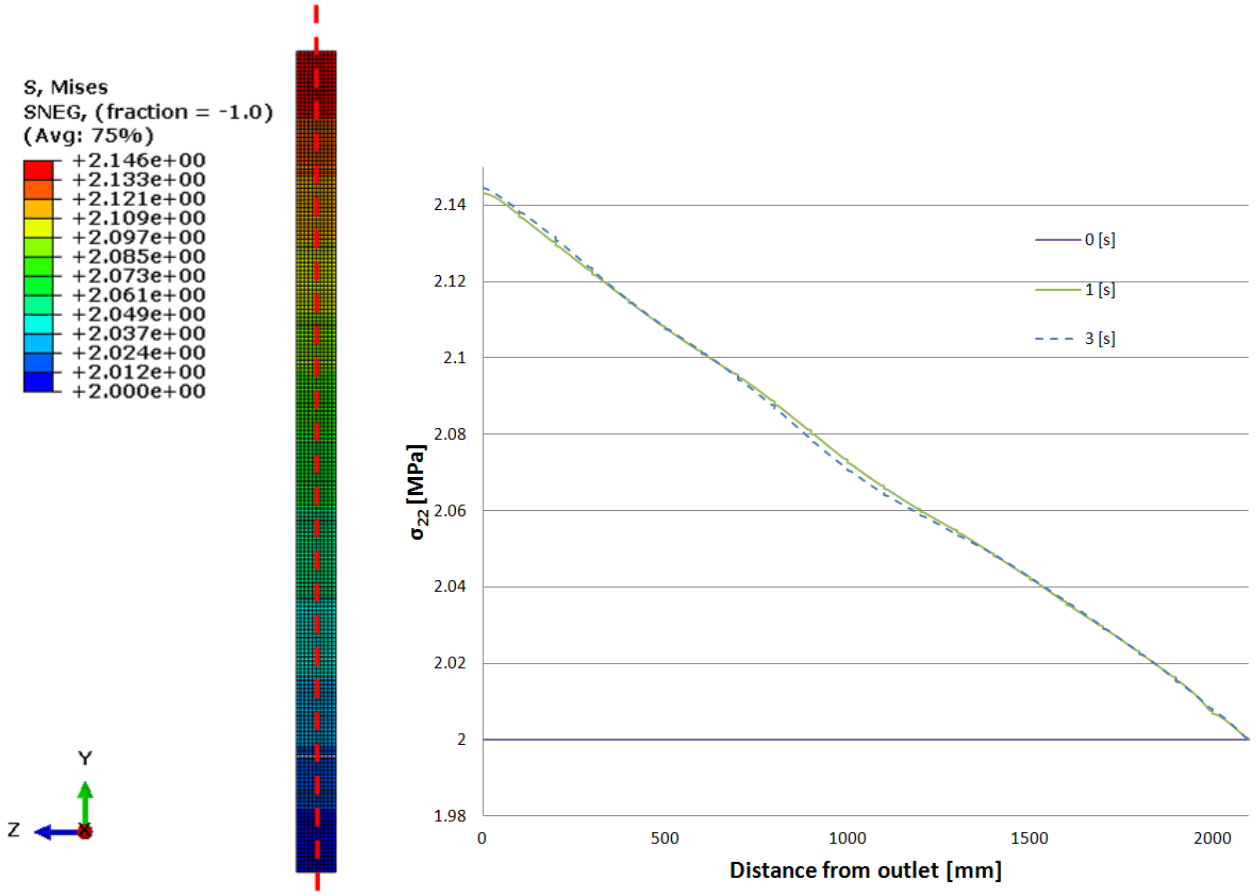

(a) The von Mises stress in the paperboard after 3000 ms

(b) The normal stress in center-cut throughout the paperboard along the y-axis, red line in 4.15a at three different simulation times; 0, 1000 and 3000 ms

Figure 4.15: Logitudinal normal stress in the paperboard when S4R elements are used

The first thing to notice is that the stress field is more stable compared to the result with S4 elements. It can be seen that the von Mises stress is increased at the outlet compared to the inlet, 2.146 and 2 MPa respectively. This difference can also be observed for the normal stress in the pure machine direction. The difference in the stress field is most likely due to the small material damping.

When enlarging the deformation in the cross direction, it is noted that the outlet edge is thinner compared to the inlet edge. One possible explanation to this result is the combination of the fixed outlet edge in cross direction, and the shuffling process. In the analysis, the outlet block is stretched resulting in a smaller inner edge. When the shuffling occurs the new, now smaller, outlet edge becomes the edge which is constrained but now with a new dimension. This will result in a tapered shape of the paperboard.

Another criterion used for validation of the model is the velocity of the paperboard which should hold 10 m/s. Figure 4.16 illustrates the velocity in machine direction for different times.

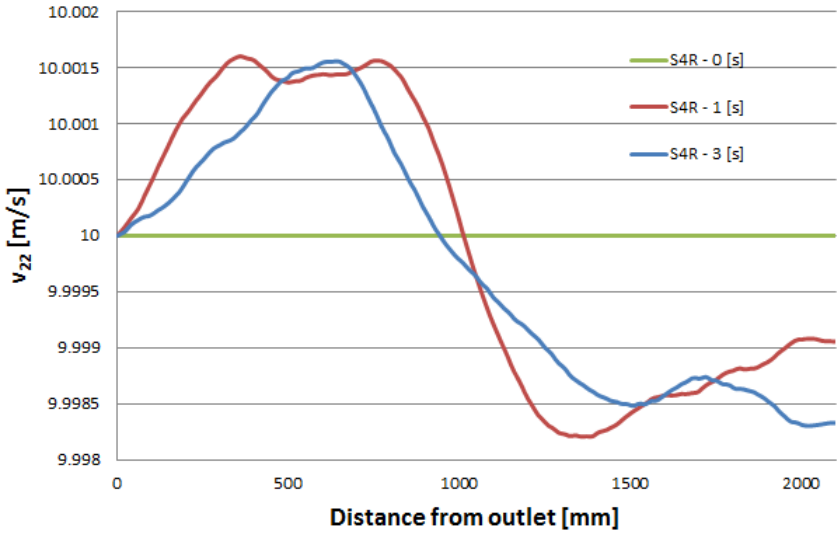

Figure 4.16: Velocity distribution in machine direction measured in a center-cut throughout the paperboard along the y-axis for different times

It is observed that the velocity is close to 10 m/s at all times. It differs only with approximately 0.018% which is assumed negligible.

When reduced integration elements are used hour glass effects can be present. The amount of artificial energy divided by the strain energy or total internal energy for the whole system should not exceed 5% for an accurate analysis according to engineering knowledge. In this model there is no artificial energy and hence no hourglass effects are present.

Since both the stresses and the velocity in the model are close to the expected result, further investigations with the periodic media model are performed.

4.2.2 Model consisting of 100 mm wide paperboard and three rollers

The next step in the periodic media analysis is to add three rollers to the paperboard model. The roller located in the center is the primary roller of interest. The upper- and lowermost rollers are created as guiders. The three rollers are modeled as analytical surfaces with a radius of 100 mm. When defining a periodic media transport with a more complex geometry as in this case, the easiest way is to first create a straight paperboard web with the rollers aligned and then move them to the desired location. The contact interactions between the paperboard and the rollers will deform the paperboard to the wanted configuration wherefore two analysis steps are performed.

The paperboard in this model consists of the same building blocks as in the simple straight model, but another 21 blocks are added resulting in a total of 42 blocks with a total length of 4.2 m. These extra blocks are needed to get the inlet and outlet of the paperboard sufficiently far away from the rollers, keeping the properties at the inlet- and outlet blocks constant throughout the analysis.

The elements used are the reduced integration elements S4R. The setup of the model is shown in Figure 4.17. The paperboard travels through the system from the bottom to the top in positive y-direction.

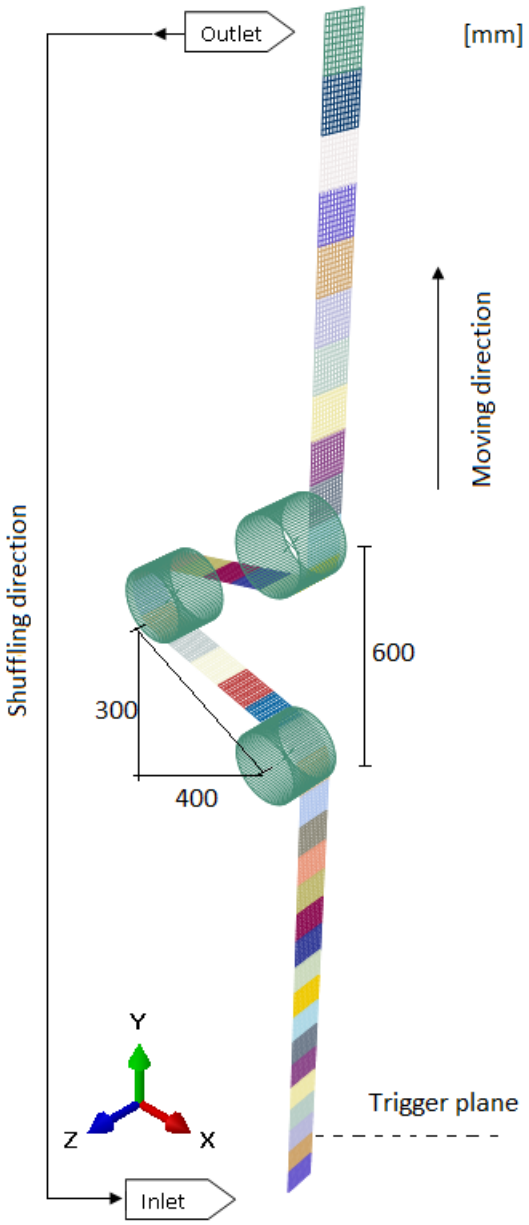

Figure 4.17: Description of the 100 mm wide paperboard model

A closer description of the two analyses

To get the 100 mm wide paperboard model, two analyses are performed. In the first analysis the rollers are positioned and a pretension in the paperboard is created. The results from the first analysis are imported and used as initial values in the second analysis together with an initial velocity of the paperboard.

In the first analysis a predefined stress of 2 MPa in machine direction is added to the paperboard and the central roller is displaced 600 mm to the left to get a position similar to the production setup. The starting position can be seen in Figure 4.18a. The displacement of the central roller is ramped with a smooth amplitude

in 500 ms to avoid large accelerations. In the same step a tension of 100 N is added at the inlet to retain the predefined stress. After the displacement of the central roller, a static step is added to reduce the dynamic effects from the first step. The outlet edge is locked and the inlet edge is free to move only in the machine direction. The final position is the configuration shown in Figure 4.18b.

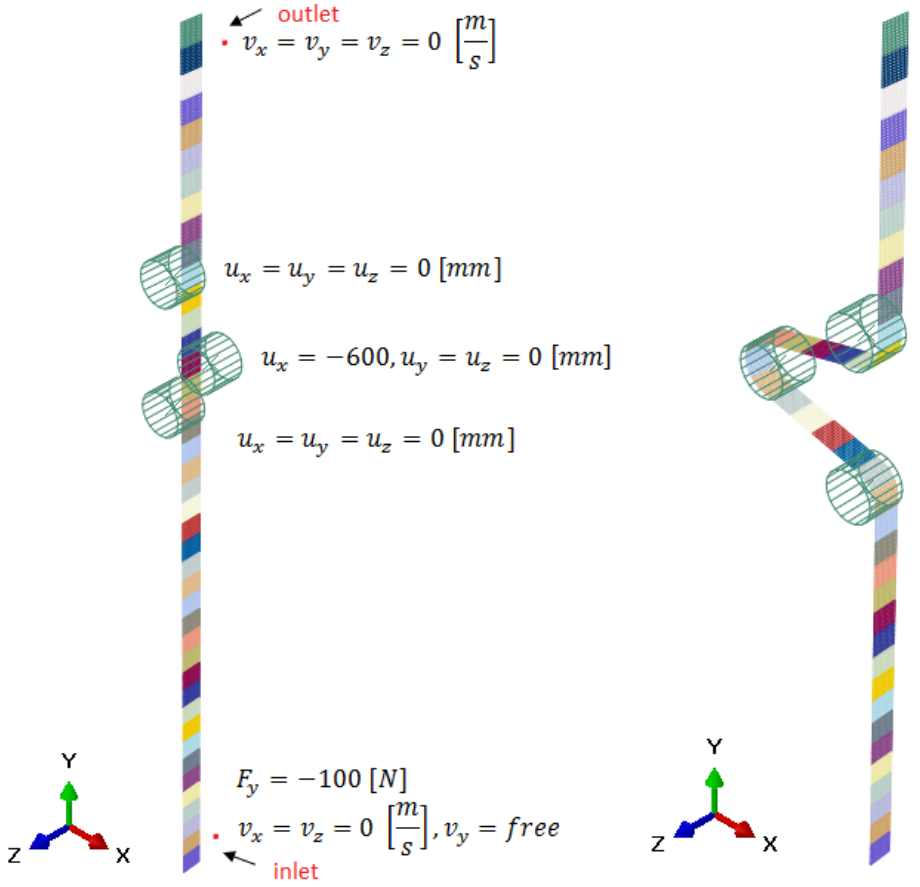

(a) Start position of the paperboard and the applied boundary conditions

(b) Results after movement of the central roller, to be imported in the second analysis

Figure 4.18: Results of the first analysis

For the second analysis, the stresses and strains are imported from the first analysis to operate as initial pretension in the paperboard. An initial velocity is applied to the paperboard by dividing it into seven sections defined in Figure 4.19, for which each of the components of the velocity are known. The velocities in sections three and five are calculated from the geometric relationship. Table 4.2 lists the velocities for the different sections.

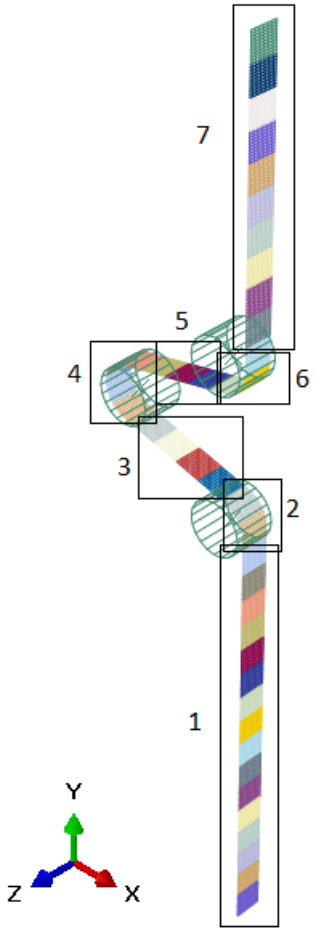

Figure 4.19: Section definitions used for the initial velocities

Table 4.2: Initial velocity defined for each section in Figure 4.19

Section number	v_x [m/s]	v_y [m/s]	ω_z [rad/ms]
1	-	10	-
2	-	-	0.1
3	-9.701	2.425	-
4	-	-	-0.1
5	9.701	2.425	-
6	-	-	0.1
7	-	10	-

Simulation of the 100 mm model without friction

To keep the velocity and the tension in the paperboard constant, the same boundary conditions and loads as in the straight paperboard model are used. The stresses in machine direction in the third section point is seen in Figure 4.20. The element size in this model is $10 \times 10 \times 0.5$ mm and the simulation time is one second.

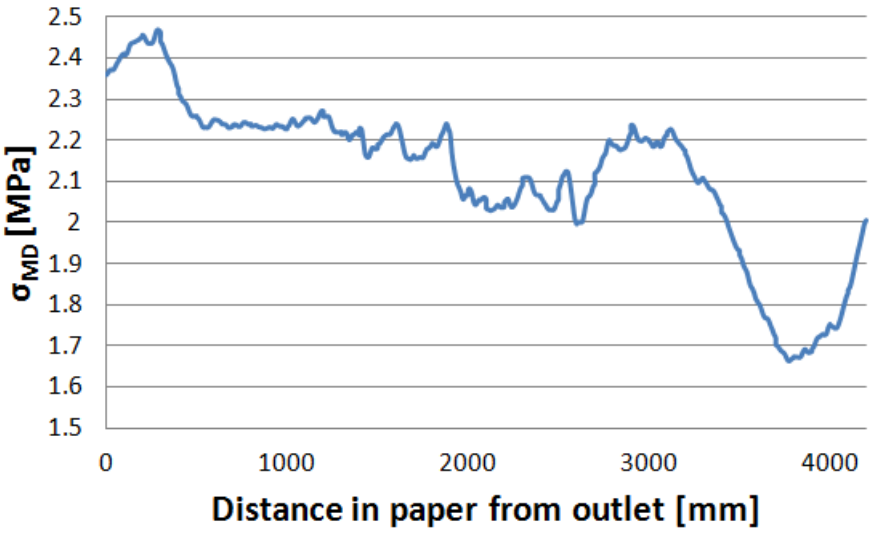

Figure 4.20: Stresses in machine direction in a center-cut throughout the paperboard along the y-axis. The stresses are taken in the third section point (in the center of the thickness of the paperboard). No friction is applied

It can be seen that the stress is fluctuating. The stres is higher at the outlet compared to the inlet, the same behavior as for the straight paperboard. The stress in machine direction varies between 2.47 and 1.66 MPa and the average stress is 2.12 MPa which is close to what is expected (6% higher).

Figure 4.21 illustrates the contact pressure over the central roller. A plot showing the contact pressure between the central roller and the paperboard is seen in Figures 4.21b.

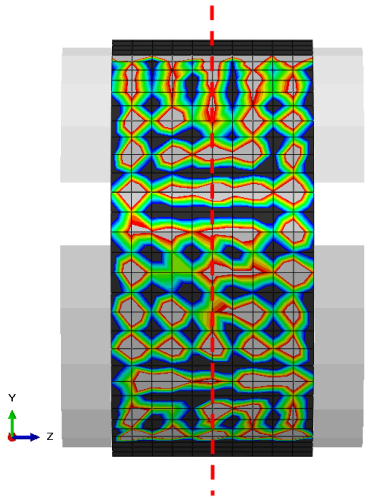

(a) The red line displays the path where the pressure is measured

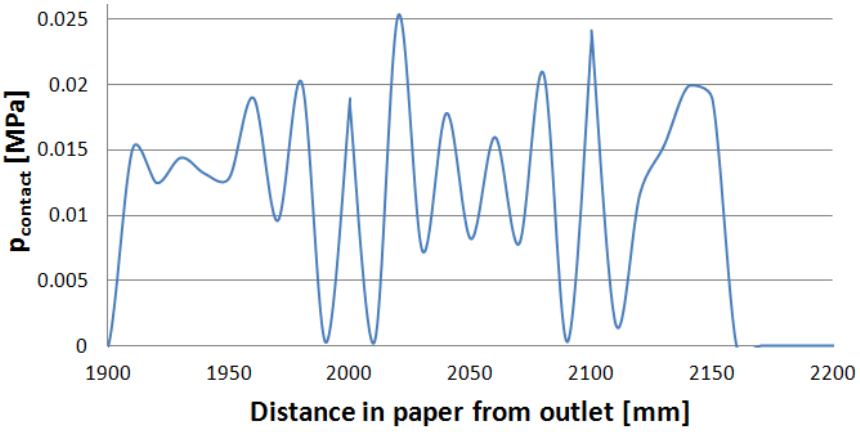

(b) The contact pressure in the middle of the central roller

Figure 4.21: Contact pressure over the central roller when no friction is applied. The values in the plot are taken at the red line in Figure 4.21a

Figure 4.21 shows a inconsistent contact pressure. The pressures are taken at a central line in machine direction of the paperboard, marked with a red line in Figure 4.21a. The average contact pressure at this line is 0.0142 MPa. This is higher than the expected analytical contact pressure which is 0.01 MPa. One explanation for this is probably due to a too coarse mesh which give rise to the uneven stress distribution. If the average is taken

for all nodes, an accurate contact pressure is received.

The hour glass effect is controlled and the artificial energy level is less than five percent of the total internal energy during the simulation, which is acceptable. This model consists of 4206 elements and 5088 nodes and it has a critical time increment of 2.20×10^{-3} ms. When using twelve CPUs the run time for a one second simulation is 10 min and 42 s.

To investigate the influence of element size an identical model consisting of half as small elements measuring $5 \times 5 \times 0.5$ mm is created. The stresses in the machine direction are identical to the results from the model with larger elements. The contact pressure shows a better result when using smaller elements. Figure 4.22 illustrates the contact pressure at the central roller for the model with smaller elements.

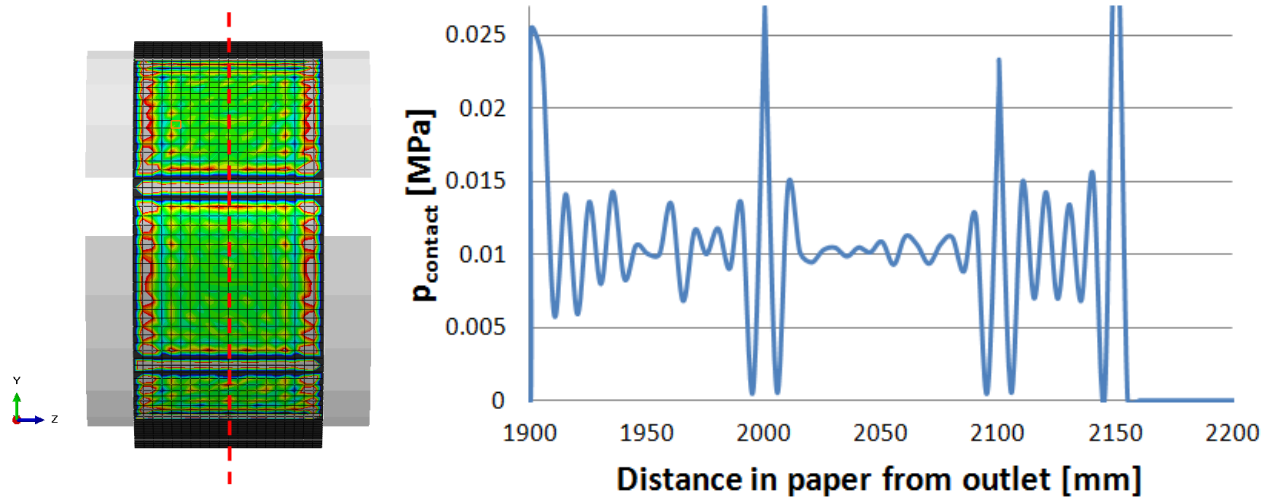

(a) The red line displays the path where the pressure is measured

(b) The contact pressure in the middle of the central roller

Figure 4.22: Contact pressure over the central roller for a model with element size $5 \times 5 \times 0.5$. *The values in the plot are taken at the red line in (a)*

Compared to the larger element model, the contact pressure is more accurate but still fluctuating. The light gray areas in Figure 4.22a are areas where the pressure is higher than 0.03 MPa which occur in the building block transition and at the outer edges. Since the building blocks are tied together the constrained elements form a larger surface area which gives rise to a higher pressure. The average pressure over the central roller is here 0.0116 MPa, which is closer to the analytical value compared to the coarser finite element model.

The artificial strain energy level is below 1% of the total internal energy in this model, meaning that the hourglass effect is, as expected, smaller in this model compared to the previous model. The critical time increment for this model is 1.05×10^{-3} ms resulting in a run time of 1 h and 28 min if the simulation time is one second. This run time is eight times longer compared to the model with larger elements. The number of elements is 16806 and the number of nodes is 18528.

Simulation of the 100 mm model with friction

The next step in the analysis is to add friction and rotation to the rollers. The used friction coefficient is 0.3. The rollers' rotational velocity corresponds to the paperboard velocity. The element size used here is $10 \times 10 \times 0.5$ mm, mainly due to the shorter calculation time. The run time for a one second simulation is for this model, 13 min and 40 s which is close to three minutes longer compared to the model without friction and rotation of the rollers. Figure 4.23 illustrates the normal stress along the machine direction in the middle of the paperboard.

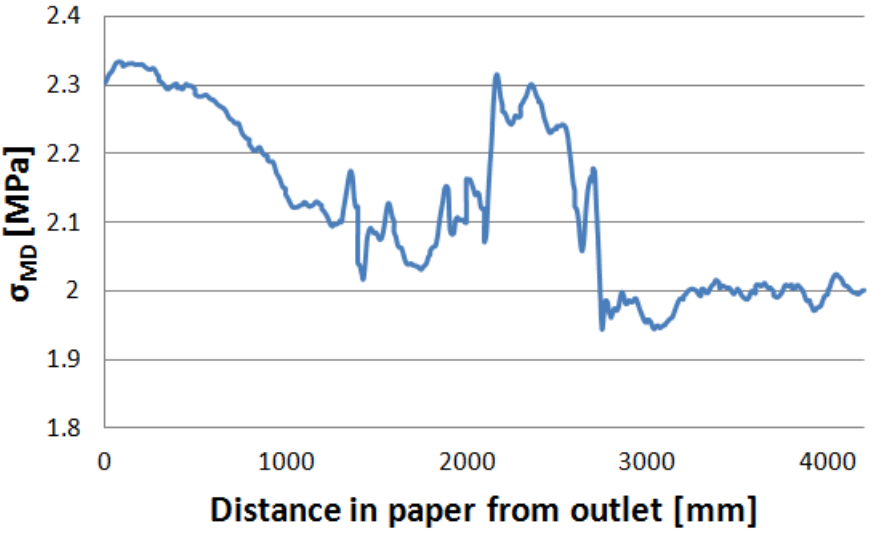

Figure 4.23: The normal stress along the y-axis (in the machine direction) in a center-cut of the paperboard. The stress values are taken at the third section point when friction is added between paperboard and rollers

This stress distribution is close to the stress distribution for the same model without friction in Figure 4.20. The average stress in the free paperboard is 2.12 MPa, just as in the frictionless model.

The contact pressure at the central roller in this model is shown in Figure 4.24 The average contact pressure in

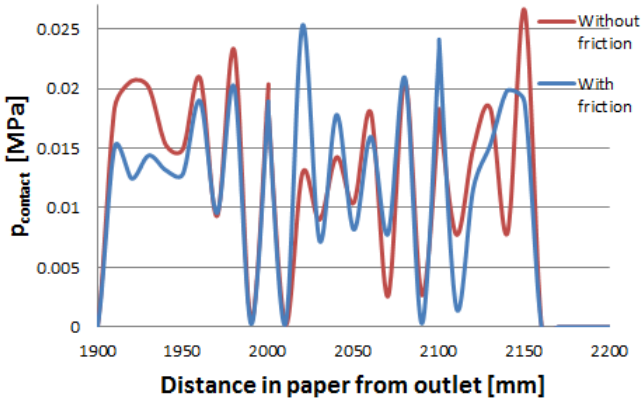

Figure 4.24: The contact pressure at the central roller where the blue line is the results with friction and the red line the results from the frictionless analysis

a cut through the middle of the paperboard in machine direction is 0.0138 MPa. Just as in the model without friction, the contact stress here is unevenly distributed but when taking the average of all nodes in contact, the contact pressure is closer to the analytical value. The artificial energy level is below 4% of the total internal energy which is lower than the model where no friction was applied.

4.2.3 Real size model consisting of 1500 mm wide paperboard and three rollers

To get a picture of how the periodic media analysis would work for the real size model, a similar model as in previous section is created but with larger dimensions of the paperboard, Figure 4.25. The same conditions are used but the dimensions of the building blocks are changed to $20 \times 1500 \times 0.5$ mm. The model consists of 23 building blocks giving a total paperboard length of 4.6 m. The element size used is $10 \times 10 \times 0.5$ mm resulting

in 69006 elements and 72939 nodes.

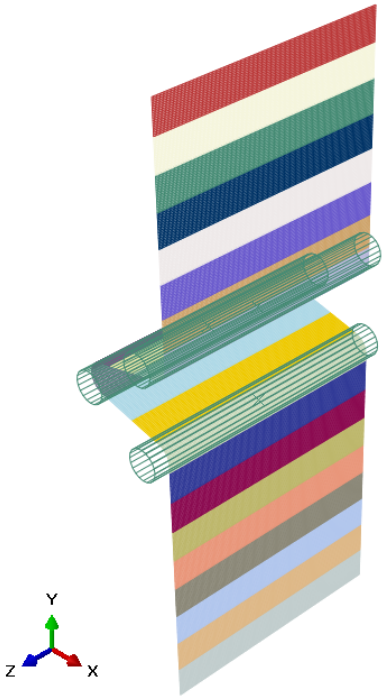

Figure 4.25: The real size model where the paperboard is 1500 mm wide

The stress variation in machine direction in the middle of the paperboard thickness (third section point) can be seen in Figure 4.26.

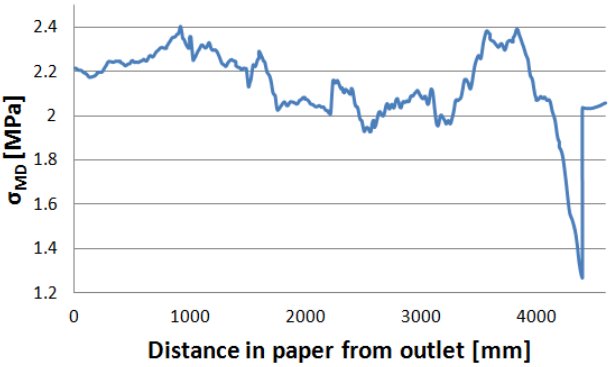

Figure 4.26: The stresses in machine direction throughout a cut in the middle of the paperboard along the y-axis. The stresses are taken in the third section point

The average stress in machine direction is 2.14 MPa which is similar to the values received in previous models.

The average contact pressure is 0.012 MPa in a cut in machine direction in the middle of the paperboard. Compared to the 100 mm model where the same element size is used, this result is closer to what is expected (0.01 MPa). There are still fluctuations between the elements which most likely will have a smaller influence if smaller elements are used.

Regarding the hour glass effect, the artificial energy level is approximately 1.2% of the total internal energy in this model. The run time of a one second simulation of the real size model is 3 h and 5 min when twelve CPUs

are used. The critical time increment is 2.20×10^{-3} ms which is the same as for the 100 mm model since the element size is the same.

4.2.4 Discussion on periodic media analysis on web handling problem

The main benefit with the periodic media analysis model is that a relatively small model can be used even for long simulations. For example, if the real size model runs for ten seconds, 100 m of paperboard will pass through the rollers. The periodic media model consists of only 4.6 m modeled paperboard, which in this case is reused ten times. If a standard Lagrangian model is to be used, that model would need to include 100 m of paperboard. The Lagrangian model would thus become more than 20 times larger resulting in a much longer run time.

One benefit the periodic media model has in comparison with the Eulerian is that it is possible to import results from previous analysis. By doing this, proper initial conditions can be applied to the model. In the models with the rollers an estimation of the initial velocity was performed and a better solution for defining velocity in machine direction is desirable.

From the first analysis of the straight paperboard, a strange behavior of the stress distribution in the paperboard could be seen where the outlet edge had deformed. This even though the velocity is locked in the cross- and thickness directions for the inlet and outlet bounds. The influence of this together with the influence of the recommended material damping should be further investigated.

Both the stresses and the contact pressure are fluctuating in all models. The normal stress in the machine direction is approximately 7% higher than expected which is needed to be taken into account. This is most likely due to the added damping. For the contact pressure it could be seen that when reducing the element size, a lower pressure closer to the analytical value was received, 0.0116 MPa compared to 0.0142 MPa. It could also be seen that the building blocks affected the contact pressure. The influence of building blocks and element sizes should be further investigated.

Since the models give inaccurate results with fluctuating stresses and contact pressures, this model is not recommended in cases when these results are of great importance. However, if the accuracy of these data are not a priority, the method displays some advantage in terms of model size and run rime. The periodic media model can therefore be recommend for cases when the paperboard is not the main part to study.

5 Analysis of thin model of lamination nip

The objective of the nip roller problem is to find the steady state contact pressure at the nip and the steady state temperature distribution throughout the rubber in the nip roller, for a thin model. These data can then be inserted in larger scale lamination simulations. Thus, a simple and computationally cheap model is sought for. For this simplified case no flow of paperboard through the nip will occur.

A hyperelastic, neo-Hookean material model is used for the rubber in the nip roller. The chill roller is made of steel and is given isotropic linear elastic material properties. The properties are shown in Table 5.1.

Table 5.1: Material properties used in the model where r is short for rubber while s is short for steel

Properties		
E_s	210 000	[MPa]
ρ_s	7.356×10^{-3}	[g/mm^3]
ν_s	0.3	
ρ_r	1.4×10^{-3}	[g/mm^3]
C_{10}	1.3925	
D_1	0.007181	

5.1 Analysis of lamination nip using the Coupled Eulerian-Lagrangian method

Since it is the nip contact pressure and the temperature distribution through the rubber that is sought for in the problem, the interesting region is around the nip. By using an Eulerian approach for modeling of the rubber, the meshing may be done in such manner that a finer mesh is achieved in the nip region while a more coarse mesh is obtained in the peripheral regions. This is allowed since the mesh is fixed in space and the rubber may flow through the mesh freely. Since the contact properties between two Eulerian materials in Abaqus are restricted, the chill roller still is modeled using a Lagrangian approach to achieve a coupled Eulerian-Lagrangian (CEL) contact problem.

The obtained CEL models are compared with a two-dimensional Lagrangian model for validation purposes. This is because the Lagrangian model gives more accurate contact properties and thus may work as a reference model. The contact pressure in the nip and the stress distribution in the rubber are compared for the two models.

5.1.1 Model description of the Eulerian modeling of the lamination nip

Figure 5.1 illustrates the initial CEL model setup. The chill roller has an outer radius of 450 mm while the outer radius of the nip roller is 118 mm. The width of the rollers is 1 mm. The material model used for the steel roller is the same as was used in previous simulations and the model parameters are listed in Table 5.1. The type of element used to model the chill roller is the Abaqus C3D8R, also previously used.

The rubber is modeled using the hyperelastic material model. The radial thickness of the rubber attached to the nio roller is 18 mm and has an inner diameter of 100 mm. When no thermal effects are taken into account, the Eulerian elements used are the EC3D8R provided in Abaqus. The element size in the radial and tangential direction in the finer mesh region is 0.25×0.25 mm. The coarse mesh is 1 mm in radial direction and 10 mm in tangential direction. The element thickness is 1 mm so the model consists of one element through the thickness.

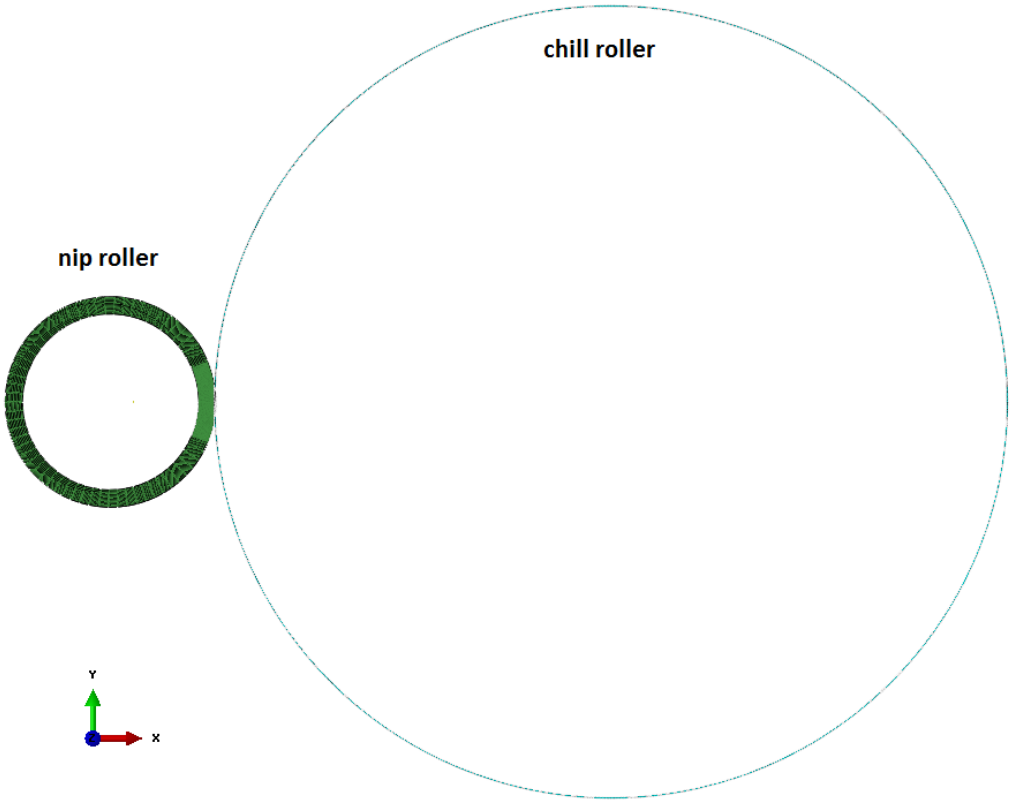

Figure 5.1: View of the lamination nip model

Figure 5.2 shows a zoomed portion of the model. It can be noted that the Eulerian elements are finer in the nip region while they are more coarse in the peripheral regions. In the figure, the volume fraction rubber is displayed as well.

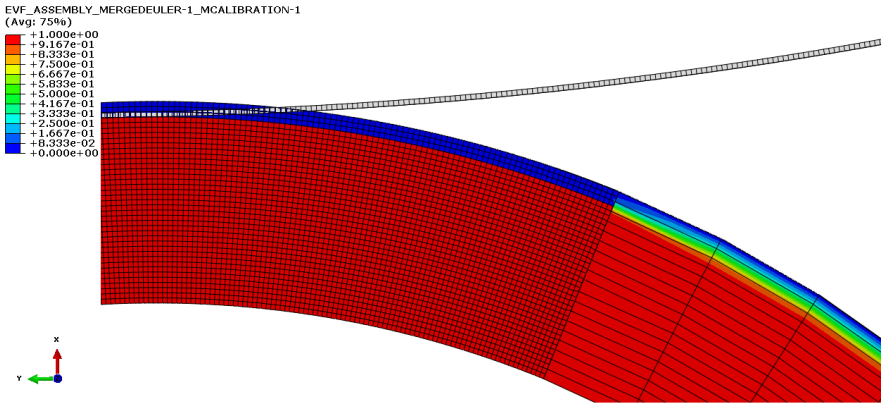

Figure 5.2: Zoomed view of the nip model, Eulerian model 1. The Eulerian mesh in the proximity of the nip is finer

Next, a second setup for the nip roller is created. The Eulerian model is then expanded to comprise a thin inner steel roller. This inner steel roller is set to be 1 mm thick in the radial direction. The Eulerian contact property between two Eulerian materials is sticky (*Abaqus Analysis User's Guide* 2014), why no slip will occur between the inner steel and the rubber. Figure 5.3 shows the steel core in this setup. For simplicity, the Eulerian model without a steel inner roller is referred to as Eulerian model 1 while the second Eulerian model described is referred to as Eulerian model 2.

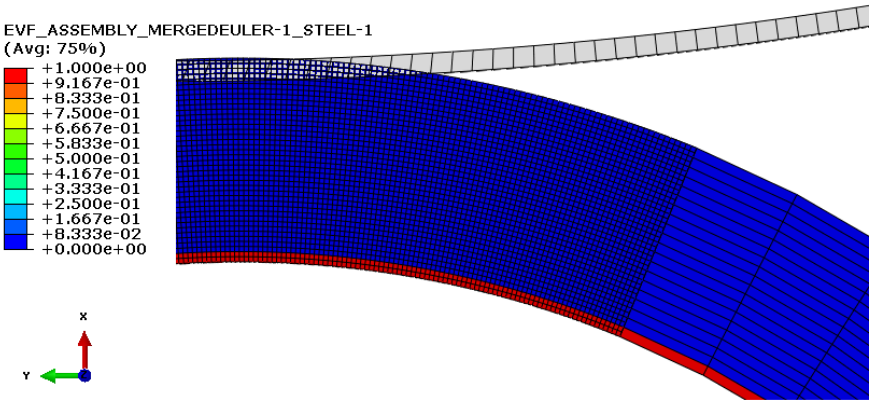

Figure 5.3: Volume fraction of the inner steel roller which is placed in the Eulerian domain of Eulerian model 2

The inner surface on the Eulerian domain is subjected to one boundary condition preventing velocities in the radial direction. This boundary condition is used on both setups, with or without an inner steel roller. In addition, no velocity in the thickness direction is allowed. Therefore, no rubber will be able to flow out of the Eulerian domain. For the whole Eulerian domain, tangential displacement is allowed so the rubber may rotate freely around its axis.

To get the nip between the nip- and chill roller, a force of 35 N is applied to the chill roller in the direction towards the nip roller. When the force is applied, the displacement of the chill roller in the x-direction is free. The chill roller is fixed in the y- and z-directions while rotation around the z-axis is allowed. Thus, the chill roller is allowed to move towards the nip roller while at the same time rotate around its axis. When creating the lamination nip in this static step, no frictional effects are present in the contact.

To get the chill- and nip roller to rotate, an angular velocity boundary condition is added to the chill roller. The rotation is ramped up and the nip roller starts to rotate due to friction. The angular velocity is of such magnitude that the tangential velocity of the outer radius of the chill roller becomes 10 m/s. When rotation of the rollers is applied, a penalty friction coefficient of 0.3 is applied in the CEL contact. In the normal direction, the default Abaqus contact is chosen.

5.1.2 Results on the lamination nip problem

In the Lagrangian reference model, a load is initially applied on the nip roller to create the lamination nip. Thereafter, a rotation on the chill roller is ramped up, and due to the friction the nip roller starts to rotate as well. The last step is steady state rotation where the angular velocity of the chill roller is held constant. Figure 5.4 shows the von Mises stress in the rubber for the Lagrangian model. Figure 5.4a displays the stress after the loading step while Figure 5.4b displays the stress at the end of the steady state rotation.

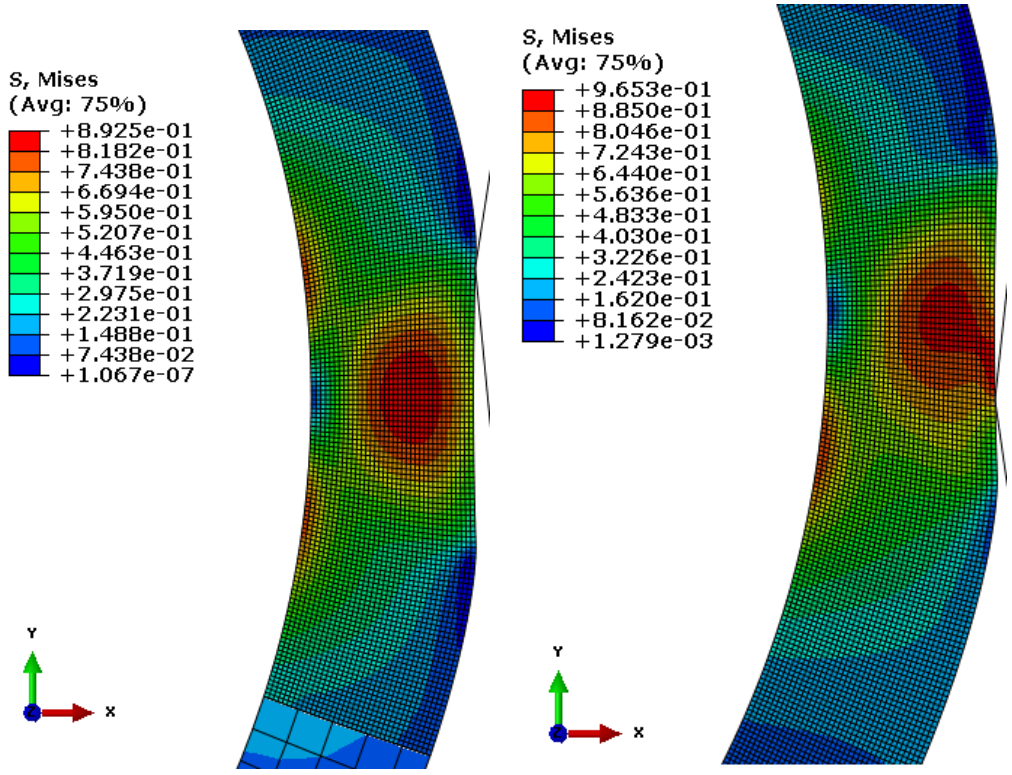

(a) σ_{vM} at the statical step *(b) σ_{vM} at the dynamic step*

Figure 5.4: σ_{vM} [MPa] in the rubber in the proximity of the lamination nip for the Lagrangian model

Results on the lamination nip problem - Eulerian model 1

The element size in the radial and tangential direction in the finer mesh region is 0.25×0.25 mm. The coarse mesh is 1 mm in radial direction and 10 mm in tangential direction. The element thickness is 1 mm so the model consists of one element through the thickness. The analysis is force controlled during the whole analysis. Initially the force is ramped up on the chill roller to create the lamination nip. When creating the lamination nip in this static step, no frictional effects are present in the contact. After the statical step, a rotation of the chill roller is ramped and thus the nip roller starts to rotate due to the friction.

Figure 5.5 presents the contact pressure obtained from the analysis of Eulerian model 1. The contact pressure obtained from the Lagrangian analysis is added for comparison. Figure 5.5a displays the obtained contact pressure after the statical step while Figure 5.5b displays the contact pressure when the rollers rotates at a steady state.

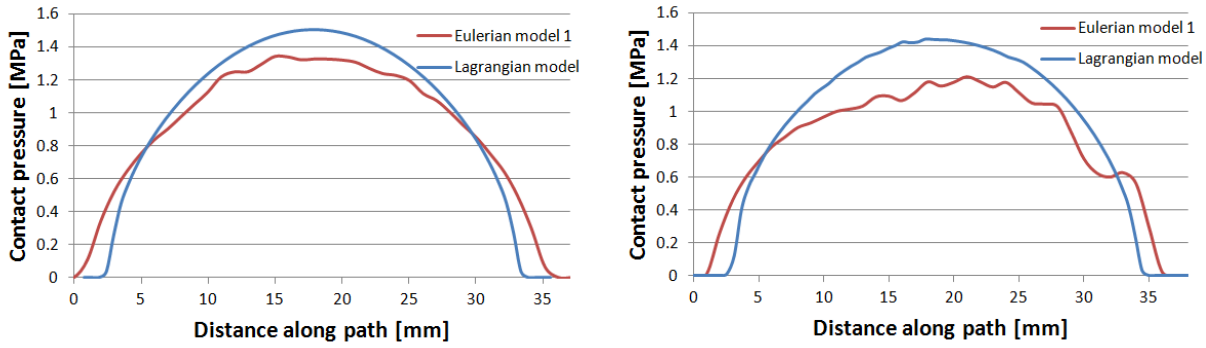

(a) Contact pressure for static nip *(b) Contact pressure for dynamic nip*

Figure 5.5: Contact pressure at the lamination nip for the Eulerian model 1 and the Lagrangian model

The contact pressure at the static step resembles the contact pressure from the Lagrangian analysis. However, the length of the contact is 4 mm wider in the Eulerian analysis and the magnitude of the contact pressure is underestimated. For the obtained contact pressure when the model is rotating, the contact length is still too wide.

The reason for that the contact length is larger for the Eulerian model 1 is mainly due to the boundary conditions on the inner surface of the rubber. In the Lagrangian model, the nodes on the inner surface are tied to a reference point in the center of the roller. Therefore, the nodes at the inner surface will move as a rigid body. That is, no relative displacement in the tangential direction on inner surface nodes is allowed. This is a reasonable constraint since in the real application, the rubber is fixed on a inner steel roller and the assumption of no slip between the rubber and inner roller is reasonable. In the Eulerian model 1 however, this rigid body condition on the inner surface nodes has not been possible to prescribe due to lack of functionality in Abaqus. Therefore, relative motion in the tangential direction is allowed on the inner surface nodes. As a consequence, the inner surface nodes close to the nip separate, and the deformation of the rubber differs in comparison with the Lagrangian model.

A setup where the inner surface nodes where given a zero velocity boundary condition in the tangential direction presented a more similar contact pressure compared with the Lagrangian model, for the static step. However, this velocity constraint has to be removed when rotation of the rollers are activated, which lead to a very inaccurate response.

The underestimation of the contact pressure may be a consequence of the CEL contact problem and the Eulerian modeling restrictions. It was shown in 3.11 that the material assignment in the Eulerian domain had a great impact on the CEL contact problem. It is hard to get a good material assignment, in terms of a high volume fraction rubber in every Eulerian element affected by the CEL contact, why the contact most likely will be underestimated.

Figure 5.6 shows the obtained von Mises stress from the Eulerian model 1 analysis. It is clear that the allowed slip on the inner surface affects the stress distribution and magnitude of the stress in the rubber significantly, when comparing the result with the Lagrangian model, see Figure 5.4.

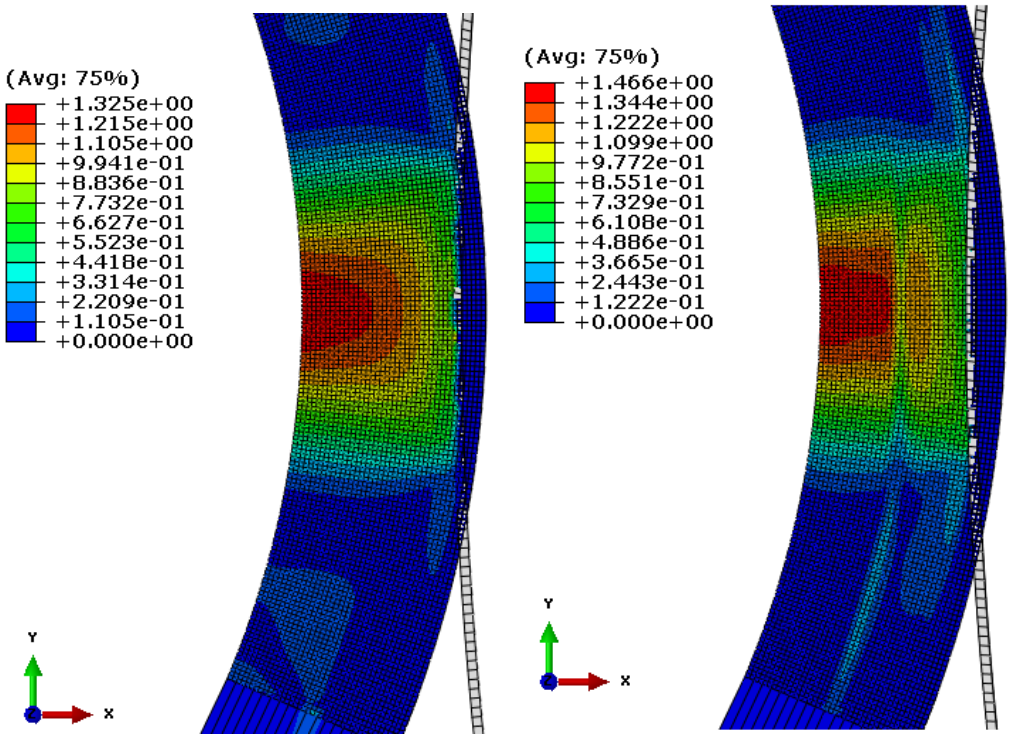

(a) Static step *(b) Dynamic step*

Figure 5.6: σ_{vM} [MPa] in the rubber in the proximity of the lamination nip for the Eulerian model 1

Results on the lamination nip problem - Eulerian 2 model

The Eulerian model 2 shows a somewhat more promising result when conducting a similar analysis. Figure 5.7 shows the obtained contact pressure after the static loading and after rotation.

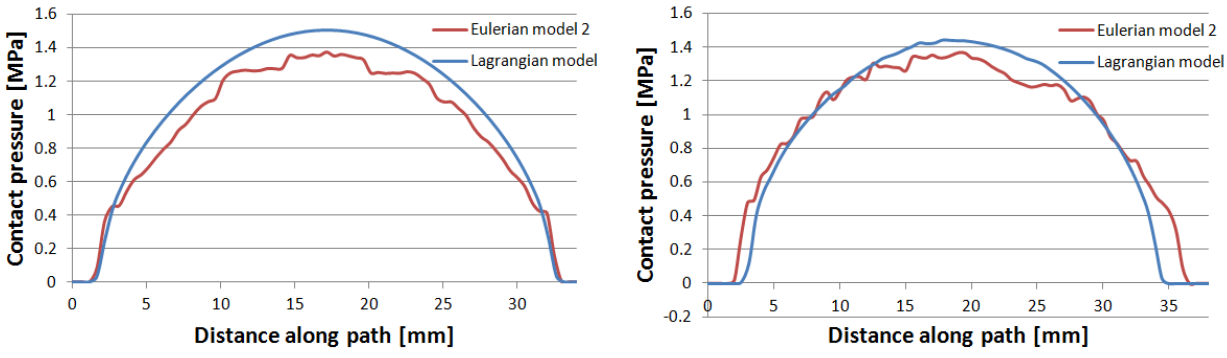

(a) Static step *(b) Dynamic step*

Figure 5.7: Contact pressure at the lamination nip for the Eulerian model 2 and the Lagrangian model

The obtained contact pressure conforms better with the contact pressure from the Lagrangian model. It may be noticed that the contact length is the same for both the Eulerian model 2 and the Lagrangian model after the static step. The achieved von Mises stress on the Eulerian model 2 are shown in Figure 5.8.

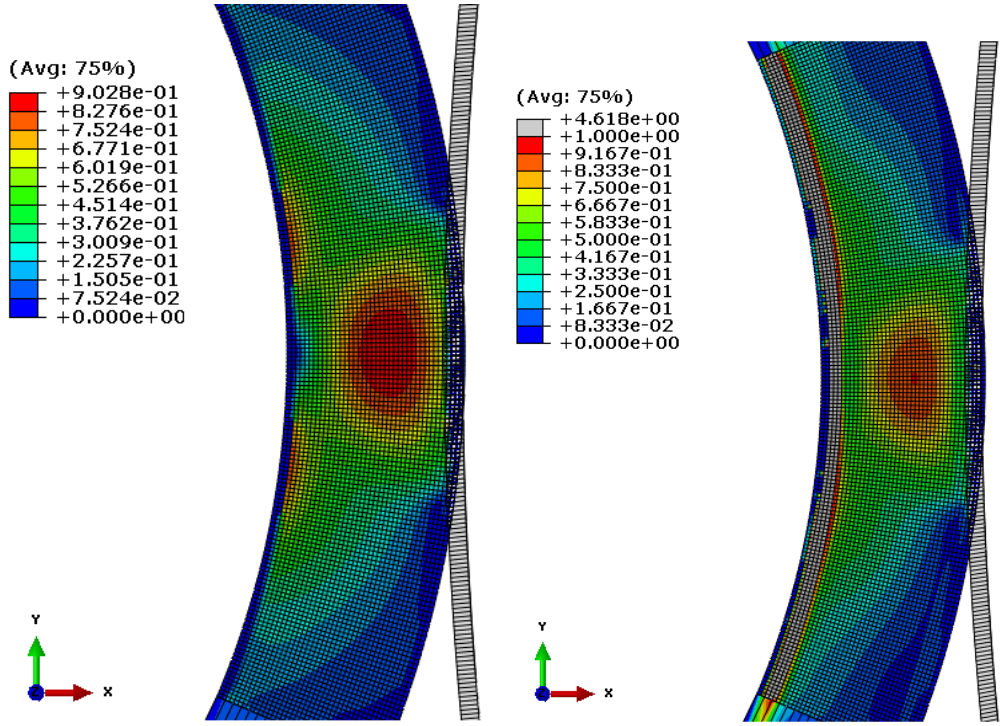

(a) Static step *(b) Dynamic step*

Figure 5.8: σ_{vM} [MPa] in the rubber in the proximity of the lamination nip for the Eulerian model 2

It is noticed that both the stress distribution and the magnitude of the stress resembles what is seen in the Lagrangian model after the static step, compare Figures 5.8a and 5.4a. High stresses in the areas where the inner steel roller and the rubber is in contact are found in the dynamic step. The magnitude of the stress is more than four times as high for the Eulerian model 2 compared to the Lagrangian reference model during the dynamic step. The cause of this might be due to high shear stresses in the sticky contact between the two Eulerian materials. The sticky contact properties are vaguely described in the Abaqus manuals and therefore it is an uncertainty in the analysis. Another reason for the higher stresses in the rubber is because the moment of inertia will increase due to the added inner steel roller.

5.1.3 Discussion on Eulerian modeling of lamination nip

Modeling the rubber using an Eulerian modeling technique allows for a fine mesh to be created in the proximity of the lamination nip while a more coarse mesh is created in the peripheral regions. However, some disadvantages are seen in the conducted analyses.

If only the rubber is modeled in an Eulerian manner, the motion of relative tangential motion of the inner surface nodes is a problem that needs to be addressed. This relative motion can be seen as a slip between the rubber and the inner steel roller in the real application, which is an unphysical behavior. The stress distribution is very much affected by this, as well as the lamination nip contact pressure.

To prevent this slip of the inner surface, an inner steel roller is added to the Eulerian domain. The sticky contact between the Eulerian rubber and Eulerian steel prevents the slip. The obtained contact pressure and stress distribution after the static step resembles the results obtained from the Lagrangian reference model. However, the stress distribution and contact pressure after the dynamic step differs more compared to the Lagrangian model.

Another aspect that needs to be taken into account is the run times. When the inner steel core is added in the

Eulerian domain, the time increment is decreased by at least a factor ten. For Eulerian model 2, the material properties of steel define the time increment instead of the rubber material properties, which define the time increment in Eulerian model 1. Hence, the run time of Eulerian model 2 is over ten times longer than the run time for Eulerian model 1. If the purpose is to achieve a simple and fast model, this is a disadvantage for Eulerian model 2 compared to Eulerian model 1.

What Eulerian model 2 shows is that if the slip on the inner rubber surface is prevented, a result similar to the Lagrangian reference model might be achieved. If it is possible to prevent this slip on Eulerian model 1 by adding some constraint on the inner surface, a model meeting the company's demands might be achieved.

6 Concluding remarks

In this project we have investigated two alternative methods for modeling web motion. The first model was based on the Eulerian method while the second model was based on the function Periodic media in Abaqus. For modeling the lamination nip the Eulerian method was used. For the web motion problem, the Periodic media analysis shows promising results which can be further investigated. The Eulerian modeling of web motion on the other hand shows weaknesses with current technology. However, for the lamination nip model the Eulerian methodology indicates capacity which is worth further study.

The main reason for not recommending further studies of the Eulerian modeling of the web motion is due to the long and expensive run times. With the existing technology, this is simply not cost-efficient. In addition to this, we also found it hard to achieve a uniform tensile stress in the paperboard. One reason for this can be the limitations in available boundary conditions, where the stresses can be obtained only by adding pressure to the edges or by displacement of the Lagrangian roller. In addition, the velocity boundary conditions necessary to constrain the paperboard movement on the inlet and outlet give rise to the high stresses in the paperboard. Figure 3.11 illustrates that it is hard to maintain a correct contact pressure when the Eulerian elements are not completely filled, which is another disadvantage with the model. The benefit with the Eulerian method is that only the area of interest needs to be model.The paperboard dimensions lead to an excessive amount of elements. The reason for this is that at least four elements through the thickness of the paperboard is recommended, leading to very small element dimensions. This resulted in a time increment for the explicit dynamic finite element simulation to be small, in the order of 1×10^{-5} ms.

Regarding the periodic media model we can conclude that because of the fluctuating stresses and contact pressure it is not recommended to model the web motion problem, where the results from the building blocks are of major interest. The fluctuations in the stress field can be seen in Figures 4.20, 4.23 and 4.26, which illustrate the stress field in machine direction for the different models. The averages of these are nevertheless close to the analytically predicted values. One benefit with the periodic media model is that it shows promising results regarding the short run times. By creating a model composed of building blocks which are reused, also the size of the model decreases significantly. One drawback with the building blocks is that they are merged together with a node-to-node tie constrain, introducing stiffness between elements that would not have been there in a standard Lagrangian mesh. The optimal size of the building block has not been investigated here, but is recommended in further studies. However, for analyses where paperboard is of secondary interest, modeling the paperboard using the periodic media function might be a good option. This will reduce the run time since the number of elements is held at a minimum for the paperboard, while at the same time an acceptable paperboard response might be achieved.

The Eulerian modeling on the lamination nip shows inconclusive results. The model allows for slip on the inner surface of the rubber, why the result differs compared to the Lagrangian reference model. When an inner steel roller was added to the Eulerian domain, the slip of the inner surface of the rubber is prevented but the run time increased significantly due to the added steel to the Eulerian domain. Furthermore, the stress distribution in the rubber for the two Eulerian models differs from the stress distribution achieved in the Lagrangian model. The main cause for this is either the slip on the rubber inner surface or the added inner steel roller in the Eulerian domain. In a thermal analysis, the stress in the rubber will affect the temperature distribution in the rubber making the difference in the stress field a concern. With this in mind, and with the limited accuracy of the coupled Eulerian-Lagrangian contact, we cannot conclude that the Eulerian modeling technique on the lamination nip is a good approach. However, if the slip on the inner rubber surface is solved, a simple model that is sufficient accurate might be achieved.

7 Recommendations and further studies

Based on the obtained results, it is not recommended to look further into the Eulerian modeling technique on the web handling problem. The periodic media analysis shows some promising results and thus it is recommended to further investigate this method, especially in models where the part modeled with periodic media is not the main concern. If modeling the paperboard a more realistic, orthotropic material model, needs to be added. Furthermore, it might be of interest to investigate how the periodic media block size affects the analysis as well. A model optimization should also be performed to improve the outcome and reduce the run time.

Another method that might be of interest to investigate regarding the web handling problem is the Arbitrarily Eulerian Lagrangian (ALE) approach. The method combines the Lagrangian and Eulerian properties by allowing some mesh motion independent of the material motion. Furthermore, in Abaqus the ALE approach allows for Eulerian inflow and outflow boundary conditions.

Regarding the lamination nip it is recommended to look further into the Eulerian technique. More realistic material models need to be added in the analysis a well as thermal properties to be able to get the temperature distribution in the rubber. It is also recommended to investigate the possibilities to get velocity controlled constraint in the model to prevent the inner surface from spreading and thereby get a more realistic result.

Another method that might be of interest to investigate regarding the lamination nip is a functionality provided in Abaqus called steady state transport analysis. The rotation of the rubber roller is then modeled as a rigid body motion and is modeled in an "Eulerian" manner letting the material flow through the mesh, while at the same time the deformation is modeled in a Lagrangian manner. Thus, the mesh is fixed in space and a finer mesh may be used close to the nip while a more coarse mesh can be used in the peripheral regions. The analyze is solved by implicit time integration in contrast to the other methods discussed, which are solved using explicit time integration.

References

ABAQUS (2005). *Abaqus, Lecture 2, Elements. Abaqus/Explicit, Advanced Topics*. URL: http://imechanica.org/files/l2-elements.pdf (visited on 11/28/2014).

Abaqus Analysis User's Guide (2014). Version 6.14. Dassault Systemès. URL: http://50.16.176.52/v6.14/index.html (visited on 11/28/2014).

Abaqus Release Notes (2014). Version 6.14. Dassault Systemès. URL: http://50.16.176.52/v6.14/books/rnb/default.htm (visited on 11/28/2014).

Abaqus Theory Guide (2014). Version 6.14. Dassault Systemès. URL: http://50.16.176.52/v6.14/books/stm/default.htm (visited on 11/28/2014).

Abaqus Verification Guide (2014). Version 6.14. Dassault Systemès. URL: http://50.16.176.52/v6.14/index.html (visited on 11/28/2014).

Abaqus/CAE User's Guide (2014). Version 6.14. Dassault Systemès. URL: http://50.16.176.52/v6.14/index.html (visited on 11/28/2014).

Benson, D. J. (1992). *Computational methods in Lagrangian and Eulerian hydrocodes*. Computer Methods in Applied Mechanics and Engineering 99 (1992) 235-394.

Benson, D. J. and S. Okazawa (Mar. 1987). *An efficient, accurate, simple ale method for nonlinear finite element programs*. Volume 72, Issue 3, Pages 305-350.

— (Dec. 2003). *Contact in a multi-material Eulerian finite element formulation*. Comput. Methods, Appl. Mech. Engrg. 193 (2004) 4277-4298.

Brolin, K. (Apr. 7, 2014). "Finite Element Method and Mathematical Models of Occupants". Powerpoint presentation. Gothenburg, Sweden.

Brown, J. (June 2009). "Two-dimensional behaviour of a thin web on a roller". *Proceedings of the tenth international conference on web handling*. IWEB.

Daping, L. and H. Yanchao (2013). *Mesh Partition Based Explicit Integration Method for Dynamic Structure FEA*, pp. 558–563.

DassaultSystemès, ed. (Nov. 13, 2014). URL: www.3ds.com (visited on 11/13/2014).

Davidson, L. (Aug. 2013). *Fluid mechanics, turbulent flow and turbulence modeling*. Gothenburg, Sweden. URL: http://www.tfd.chalmers.se/~lada/MoF/lecture_notes.html (visited on 11/07/2014).

Draganis, A. (2014). "Numerical simulation of thermomechanically coupled transient rolling contact - An arbitrary Lagrangian-Eulerian approach". PhD thesis. Department of Applied Mechanics.

Ghosh, S. and N. Kikuchi (1991). *An arbitrary Lagrangian-Eulerian finite element method for large deformation analysis of elastic-viscoplastic solids*, pp. 127–188.

Hibbitt, H. and B. Karlsson (Nov. 1979). *Analysis of pipe whip*. Report EPRI-NP–1208 to Electric Power Research Institute. INIS Volume 11, Issue 14. Ref. Number 11538109.

Irgens, F. (2008). *Continuum Mechanics*. Springer Berlin Heidelberg. ISBN: 978-3-540-74297-5.

Milkunleashed, ed. (2014). *How uht milk works*. URL: http://www.milkunleashed.com/shelf-safe-milk/aseptic-packaging-uht-milk.html (visited on 12/19/2014).

Orcina, ed. (Dec. 1, 2014a). *Rayleigh Damping*. OrcaFlex. URL: http://www.orcina.com/SoftwareProducts/OrcaFlex/Documentation/Help/Content/html/RayleighDamping.htm (visited on 12/01/2014).

— ed. (Dec. 1, 2014b). *Rayleigh Damping: Guidence*. OrcaFlex. URL: http://www.orcina.com/SoftwareProducts/OrcaFlex/Documentation/Help/Content/html/RayleighDamping,Guidance.htm (visited on 12/01/2014).

Ottosen, N. and H. Petersson (1992). *Introduction to the finite element method*. Pearson Education Limited/Pearson Prentice Hall. ISBN: 0-13-473877-2.

Sun, J., K. Lee, and H. Lee (Apr. 1999). *Comparison of implicit and Explicit finite element methods for dynamic problems*. Journal of Materials Processing Technology 105 (2000) 110-118.

Vedmar, L. (1998). *Maskinelement. Transmissioner*. Lund, Sweden: Lunds Tekniska Högskola.

Wing Kam Liu, T. B. and H. Chang (Oct. 1986). *An arbitrary lagrangian-eulerian finite element method for path-dependent materials*. Volume 58, Issue 2, Pages 227-245.

Yongsheng Qi, F. Z. and J. Zhou (2013). *Applications of Explicit FEA in Structural Static and Dynamic Analyses*, pp. 1498–1501.

Zienkiewicz, O. C. and R. L. Taylor (1991a). *The Finite Element Method. Vol. 1. Basic formulation and linear problems*. 4th. McGRAW-HILL Book Company (UK) Limited. ISBN: 0-07-084174-8.

— (1991b). *The Finite Element Method. Vol. 2. Solid and fluid mechanics Dynamics and non-linearity*. 4th. McGRAW-HILL Book Company (UK) Limited. ISBN: 0-07-084175-6.